mini-MEndR: A miniaturized 96-well predictive assay to evaluate muscle stem cell mediated repair

Nitya Gulati[1,2†], Sadegh Davoudi[2,3†], Bin Xu[2,3†], Saifedine T. Rjaibi[1-3‡], Erik Jacques[2,3‡], Justin Pham[1,2], Amir Fard[1-3], Alison P. McGuigan[1,3*], Penney M. Gilbert[2-4*]

[1] Department of Chemical Engineering and Applied Chemistry, University of Toronto, Toronto, ON, M5S3E4, Canada

[2] Donnelly Centre, University of Toronto, Toronto, ON M5S3E1, Canada

[3] Institute of Biomedical Engineering, University of Toronto, Toronto, ON, M5S3G9, Canada

[4] Department of Cell and Systems Biology, University of Toronto, Toronto, ON M5S3G5, Canada

[*] Co-corresponding author e-mails: alison.mcguigan@utoronto.ca (A.P.M.) and penney.gilbert@utoronto.ca (P.M.G.)

[†] These authors contributed equally to this work.

[‡] These authors contributed equally to this work.

Abstract

Functional evaluation of novel molecules that promote stem cell mediated endogenous repair often require multiplexed *in vivo* transplant studies that are low throughput and hinder the rate of discovery. Here, we optimized and miniaturized a previously developed muscle endogenous repair (MEndR) *in vitro* assay that captures significant events of *in vivo* muscle endogenous repair to offer greater throughput for functional validation studies. The mini-MEndR assay consists of miniaturized cellulose scaffolds designed to fit in 96-well plates, the pores of which are infiltrated with myoblasts encapsulated in a fibrin-based hydrogel to form engineered skeletal muscle tissues. Pre-adsorbing thrombin to the cellulose scaffolds facilitates *in situ* tissue polymerization, a critical modification that enables new users to rapidly acquire assay expertise. Following the generation of the 3D myotube template, muscle stem cells (MuSCs), prospectively isolated from mouse skeletal muscle tissue, are engrafted onto the engineered template. A regenerative milieu is then introduced by injuring the muscle tissue with a myotoxin. We evaluated two different commercially available human primary myoblast lines and were able to successfully generate miniaturized 3D muscle templates, as well as recapitulate the *in vivo* outcomes of a known modulator of MuSC mediated repair but only in the presence of both the stem cells and the regenerative milieu. Thus, the mini-MEndR culture assay captures the ability of different molecular treatments to modulate donor MuSC skeletal muscle production and niche repopulation. The miniaturized predictive assay offers a simple, scaled platform with which to investigate MuSC endogenous repair molecular modulators, and thus is a promising strategy to accelerate the muscle endogenous repair discovery pipeline.

Key Words: predictive assay, scale-up, manufacturing, skeletal muscle, stem cell, endogenous repair

62 **Introduction**

63 The regenerative capacity of healthy skeletal muscle is driven by the activity of tissue resident
64 muscle stem cells (MuSCs). With age[1], or in disease, e.g. Duchenne muscular dystrophy (DMD)[2,3],
65 MuSCs remain present, but have diminished repair capabilities. Therapeutic strategies to correct
66 diminished skeletal muscle endogenous repair have a growing need. One exciting emerging
67 strategy to improve skeletal muscle endogenous repair is the use of drugs to boost MuSC function
68 (i.e. endogenous repair), for which pre-clinical studies in mice demonstrate the promise of this
69 therapeutic approach[3–6].

70 A current gold standard assay to determine whether a molecular target restores MuSC
71 function, and thus to make a go/no-go decision in the discovery process, is the intramuscular
72 transplantation assay[7–9]. This assay involves transplanting treated cells into the pre-irradiated and
73 pre-injured hindlimb of immune-compromised rodents and then assessing the capacity of the
74 transplanted cell population to make muscle and repopulate the stem cell compartment. This gold-
75 standard assay is expensive, low throughput and plagued by high variation, which in turn limits
76 the number of candidates that can be tested. To overcome this pain point in the discovery process,
77 we invented MEndR, an in vitro functional assay that predicts skeletal muscle endogenous repair
78 outcomes in a dish[10]. MEndR is a lower cost alternative to the intramuscular transplantation assay
79 that enables both molecule screening and functional validation in a single test.

80 In the MEndR culture assay, we first engineer thin sheets of mature skeletal muscle tissue
81 by infiltrating a thin cellulose (paper) scaffold with primary patient-derived muscle progenitor
82 cells encapsulated in an extracellular matrix hydrogel. MuSCs freshly isolated from mouse
83 hindlimb skeletal muscle tissue are labelled and then incorporated into the 3D muscle sheets.
84 Shortly thereafter, the muscle tissue sheet is injured by exposure to a myotoxin to induce a
85 regenerative microenvironment, and MuSC-mediated muscle tissue template repair is assessed
86 phenotypically by assessing the contribution of labelled MuSCs to new muscle tissue formation,
87 and to niche repopulation, using fluorescent image analysis. To validate the predictability of our
88 platform, we tested a number of drugs that were previously reported modulators of MuSC function
89 and compared results using MEndR with those we obtained in parallel using the *in vivo*
90 transplantation assay. MEndR accurately predicted *in vivo* transplantation assay outcomes. Side-
91 by-side comparisons accurately identified a range of repair phenotypes observed in the *in vivo*
92 transplantation assay results. Furthermore, since MEndR is an in vitro platform, the user has

93 greater control over the conditions during drug testing (e.g., media composition, state of the
94 template, uniform exposure to the myotoxin injury agent) to potentially improve reproducibility.
95 With this we demonstrated, for the first time, the ability to compress the translational pipeline by
96 offering an alternative to the *in vivo* validation assay that is, in theory, amenable to testing all 2D
97 drug screen 'hits' without the need for biased pre-selection.
98 The MEndR functional assay is poised to serve as a secondary screen service to prioritize
99 'hits' arising from high-throughput screens designed to discover MuSC potency modulators.
100 However, MEndR assay scale-up from a 24-well footprint to a 96-well format is critical to realizing
101 this goal. Candidate assessment performed in a 96-well format has the potential to offer an order
102 of magnitude higher throughput than the intramuscular transplantation assay. Towards this goal,
103 we herein describe the scaling of the MEndR assay into a 96-well footprint and we validate that
104 the miniaturized platform captures all stem cell functional metrics shown in the original MEndR
105 platform.
106
107 **Materials and Methods**
108 **Human myoblast maintenance and 2D differentiation**
109 Human primary myoblasts (pMB) were purchased from Cook MyoSite® (Table 1). For routine
110 culture, myoblasts were plated on collagen-coated tissue culture plates (Table 2) at a seeding
111 density of 5000 - 7500 cells/cm^2. Myoblasts were maintained in human pMB growth medium
112 (GM; Table 2) and passaged using trypsin upon reaching ~70% confluency. Culture media was
113 replaced every other day. Myoblasts were used at passage 6-7 for 2D experiments, and at passage
114 8 in all 3D tissue experiments. For 2D differentiation studies, myoblasts were plated at a seeding
115 density of ~37,000 cells/cm^2 on Geltrex™ coated plates in human pMB GM. The cultures were
116 transitioned to 2D differentiation media (DM; Table 2) one-day post seeding to induce fusion. Half
117 of the DM was removed and replaced every other day. Cultures were fixed and analyzed on day 9
118 of differentiation.
119
120 **MEndR and mini-MEndR myotube template fabrication and injury**
121 24-well plate format myotube templates were generated as previously described by our group[10].
122 Briefly, rectangle patterns with 0.5 cm x 1 cm dimensions were printed onto the cellulose scaffold
123 product (MiniMinit® Products Ltd) with a LaserJet printer and then cut into individual rectangular

124 scaffolds with scissors. These scaffolds were then autoclaved in a dry cycle to maintain sterility.
125 To generate the myotube templates, sterile cellulose scaffolds were carefully placed on a custom
126 polydimethylsiloxane (PDMS) block using a pair of sterile tweezers. The PDMS block was placed
127 in an ethanol-sterilized plastic container with moist paper on the bottom and a tight-fitting lid to
128 seal the top, to create a humidified chamber. Next, a fibrinogen solution (Table 2) was freshly
129 prepared and filter-sterilized with a 0.22 µm filter. pMBs were resuspended at a concentration of
130 (3.33E+07 cells/mL) in an extracellular matrix (ECM) master mix (Table 2). 100 U/mL of
131 thrombin (Sigma, #T6884) was added to the pMB/ECM mixture to achieve a final concentration
132 of 0.225 U/mg of fibrinogen. The mixture was maintained on ice throughout. Next, 12 µL of
133 pMB/ECM mixture (i.e., 4.0E+05 pMBs) was evenly distributed onto the cellulose scaffolds using
134 a custom spreading tool[11]. The humidified chamber was then sealed with the lid and incubated at
135 37 °C for 5 minutes to encourage conversion of fibrinogen to fibrin clots. Next, MEndR GM (Table
136 2) was gently pipetted onto each of the scaffolds to facilitate easy detachment from the PDMS
137 block. The scaffolds were then gently lifted and placed into individual wells of a 24-well plate
138 containing 1 mL of MEndR GM. Two days later, the GM was removed and replaced with MEndR
139 DM to facilitate myotube differentiation. Half of the MEndR DM was removed and replaced every
140 other day.

141 For 96-well plate format myotube templates (mini-myotube templates), cellulose paper
142 (MiniMinit® Products Ltd) was cut into circular discs using a 5 mm biopsy punch (Integra,
143 #MLT3335) and subsequently sterilized in an autoclave. 96-well plates (PhenoPlate 96-well
144 microplates, PerkinElmer) were prepared for tissue seeding and culture by treatment with 100 µl
145 of 5 % Pluronic F-127 (Sigma, Cat#P2443) solution in dH_2O (Table 2) at 4 °C overnight, or
146 minimum one hour, which served to create a non-adhesive surface to prevent cell attachment on
147 the plates and facilitate tissue self-organization. The pluronic acid was then aspirated, and the plate
148 was left to dry in the biosafety cabinet with the lid removed until the thin film of liquid could no
149 longer be visualized (~20 min). The autoclaved disks were then placed in the center of the
150 corresponding wells of the 96-well plate using a sterile anti-static tweezer. Next, a 0.8 U/mL
151 thrombin solution was prepared by diluting the 100 U/mL thrombin stock in PBS, and 4 µL of the
152 0.8 U/mL thrombin solution was dispensed onto the center of each paper disc. The discs were then
153 left to dry in the biosafety cabinet. Meanwhile, a 10 mg/mL fibrinogen solution (Table 2) was
154 freshly prepared by dissolving lyophilized fibrinogen powder in 0.9 % wt./vol of NaCl solution,

155 and subsequently sterilized by passing through a 0.22 µm filter. pMBs were trypsinized, counted
156 and suspended in ECM master mix (Table 2) at a concentration of 2.5E+07 cells/mL, which was
157 kept on ice. Next, 4 µL of pMB/ECM mixture (i.e., 1.0E+05 pMBs) was pipetted into the center
158 of paper discs with pre-adsorbed thrombin, with the mixture entering the cellulose scaffold pores
159 by capillary action. Cellulose scaffolds impregnated with pMB/ECM were incubated for 5 minutes
160 at 37 °C. 200 µL of MEndR GM (Table 2) was then gently pipetted into each well, ensuring that
161 the tissues did not flip over. The 96-well plate was then returned to the cell culture incubator (37
162 °C, 5 % CO_2). The next day, tissues that failed to detach from the bottom of the well (by visual
163 inspection), were released by gently triturating the culture media in the well with a p200 pipette.
164 Two days later, the MEndR GM was aspirated and replaced with MEndR DM (Table 2). Half of
165 the MEndR DM was removed and replaced with fresh medium every other day.
166
167 **Immunohistochemistry**
168 2D myotube cultures, and 3D muscle tissues, were harvested and fixed at the indicated culture
169 endpoints by removing the media, washing gently three times with phosphate buffered saline
170 (PBS), and then incubating in 200 µL of 4% paraformaldehyde for 15 min at room temperature.
171 The samples were washed three times with PBS every 5 min followed by incubation in blocking
172 solution (Table 3) overnight at 4 °C, or for 1 hr at room temperature. Following blocking, which
173 also contains permeabilization agent, samples were then incubated with 40 µL of primary
174 antibodies (Table 3) diluted in PBS and 0.1 % goat serum, overnight at 4 °C. Next, the samples
175 were washed three times with cold PBS every 10 min and then incubated for 45-60 min at room
176 temperature with 40 µL of a secondary antibody mix (Table 3), containing DRAQ5 nuclear counter
177 stain (Table 3), and diluted in PBS with 0.1% goat serum. The secondary antibody mix contained
178 phalloidin conjugates (Table 3) for the experiments where phalloidin coverage was assessed. The
179 samples were then washed three times with cold PBS. Tissue samples were stored in PBS at 4 °C
180 until image acquisition.
181
182 **Image acquisition**
183 Confocal z-stack images of immunostained samples were acquired using an Olympus FV-1000
184 confocal microscope and Olympus FluoView V4.2b imaging software. Images were acquired
185 using x4 (0.13 NA), x10 (0.3 NA) or x20 (0.45 NA) air objectives (Olympus) and the step size for

186 each z-stack image acquired was set at the optimal value for each objective by the imaging
187 software. Laser power, PMT HV and background offset were adjusted using the grey scale scan.
188 Laser power was set lower than 75 % during image acquisition to prevent photobleaching and
189 reduce cytotoxicity for all images. Next, laser power and HV were adjusted to avoid overexposure
190 and saturation as guided by the red pixels. Background offset was adjusted to preclude blue pixels
191 in each of the stacks. HV was set lower than 750 to reduce noise and Gain was set at 1 for all
192 images. For the niche repopulation experiments, tissues were imaged using an Opera Phenix High
193 Content Screening system outfitted with a x20 water immersion objective. Confocal stacks were
194 converted to the 2D space using a maximum Z-projection prior to image analysis. Nuclear fusion
195 index, $Pax7^+$ cell enumerations, as well as sarcomeric α-actinin (SAA), green or yellow fluorescent
196 protein (GFP/YFP) or phalloidin tissue coverage were quantified exactly as we previously
197 described[10].
198
199 **Bead retention assay and analysis**
200 Cellulose-based paper scaffolds (MiniMinit® Products Ltd) were cut using a 5 mm diameter
201 biopsy puncher and placed in a 96-well plate. Scaffolds were pre-adsorbed with thrombin at a
202 concentration of 0.8 U/ml (0.2 U/mg fibrinogen) and allowed to dry for one hour in the biological
203 safety cabinet with the 96-well plate lid removed. Next, a Master Mix was prepared by diluting 15
204 μm diameter fluorescent beads (Bangslab, #FCDG011) 10 times in ECM master mix (Table 2).
205 Then, 4 μL of the bead MasterMix was infiltrated into each of the dried scaffolds and the scaffolds
206 were subsequently incubated at 37 °C for 5-10 min to allow the Master Mix and thrombin to gel.
207 The scaffolds were imaged using confocal microscopy (Olympus FV-1000, x4 air
208 objective, laser power 20-40 %, HV < 700) to determine the initial number of beads. Scaffolds
209 were maintained in PBS while not being imaged to prevent them from drying. After the initial
210 images were captured, scaffolds were washed with PBS three times to mimic the turbulence
211 experienced by scaffolds during 3D culture (e.g., media changes). The scaffolds were imaged once
212 more, using the same settings, to determine the number of beads retained.
213 To quantify the number of beads in an image, confocal stacks were first converted to the
214 2D space using a maximum Z-projection. Thresholding was performed using FIJI's built-in Yen
215 algorithm to binarize the image into fluorescent beads and background. Overlapping adjacent

216 beads were segmented using the watershed tool. Finally, FIJI's *Analyze Particles* function was
217 used to count the number of beads recorded in the image.
218
219 **Mini-myotube template endogenous repair**
220 To study myotube template endogenous repair potential, we optimized an injury protocol that
221 achieved an ~50 % reduction in SAA coverage of the myotube template post injury. Specifically,
222 the culture media was removed from the myotube template tissues and replaced with MEndR DM
223 containing 0.5 µM cardiotoxin (CTX) (Latoxan #L8102 – diluted in water) on day 7 of
224 differentiation. Tissues were incubated on an orbital shaker in a 37 °C incubator for 4 hours. The
225 medium was gently pipetted at the 2-hour mark to encourage the movement of the medium in the
226 well and the detachment of any broken fibers. After the 4-hour incubation, cardiotoxin was
227 removed by gently washing the tissues twice with MEndR DM. Tissues were then cultured in
228 MEndR DM supplemented with 5 ng/mL rh-FGF2 for 24 hr, to assess template injury.
229 For myotube template self-repair studies, tissues were first cultured for a period of 5 days
230 post injury, during which time the tissues were treated with endogenous repair stimulating drugs
231 as indicated in Table 4. The MEndR DM supplemented with FGF2 and drugs was completely
232 replaced every other day. For the remaining duration of the assay, tissues were cultured in MEndR
233 DM and half of the media was replaced every other day.
234
235 **Mouse strains and ethics**
236 All animal use protocols were reviewed and approved by the local Animal Care Committee (ACC)
237 within the Division of Comparative Medicine (DCM) at the University of Toronto. All methods in
238 this study were conducted as described in the approved animal use protocols (#20012838) and
239 more broadly in accordance with the guidelines and regulations of the DCM ACC and the
240 Canadian Council on Animal Care. 129-Tg(CAG-EYFP)/7AC5Nagy/J mice are maintained by
241 crossing homozygous males and females. C57BL/6-Tg (CAG-EGFP)1Osb/J (Actin-eGFP) mice
242 were purchased from the Jackson Laboratory (USA) and utilized in experiments after a 1-week
243 acclimatization period. Tg(Pax7-nGFP) mice[12] were a kind gift from Dr. Shahragim Tajbakhsh,
244 transferred from the laboratory of Dr. Michael Rudnicki and maintained at the University of
245 Toronto by backcrossing to C57Bl/10ScSn (Jackson Laboratory) and genotyping for the GFP gene.
246 For all experiments, 8-12 weeks old female mice were used.

247

248 **Murine muscle stem cell (MuSC) isolation**

249 MuSCs were prospectively isolated from the collective mouse hindlimb muscles using
250 Fluorescence Activated Cell Sorting (FACS) as previously described[13]. Briefly, mice were
251 humanely euthanized, and their hindlimb muscles were removed and placed in a GentleMACS
252 dissociation tube (Miltenyi Biotec, #130-096-334) containing Type 1A Collagenase (628 U/mL,
253 Sigma, #C9891) in DMEM. The tissue was then physically dissociated by running the "Skeletal
254 Muscle" program in the GentleMACS Dissociator (Miltenyi Biotec, #130-093-235). Next, the tube
255 was placed on a rotating mixer at 37 °C for 1 hr. Dispase II (0.04 U/mL, Life Technologies,
256 #17105041) was then added to the tube and the muscle was further dissociated by passing through
257 a 10 mL pipette 10 times. Afterwards, the tube was returned to the rotating mixer for 1 hr. Next,
258 the digested muscle was passed through a 21 G needle 10 times, after which 10 mL of FACS buffer
259 was added to the tube. The digested muscle was passed through a 70 µm cell strainer, followed by
260 a 40 µm cell strainer. The resulting cell slurry was centrifuged at 400 g for 15 min, after which the
261 pellet was resuspended in 1 mL of FACS buffer. Red blood cells were removed by resuspending
262 the cell pellet in red blood cell lysis buffer and incubating at room temperature for 7 min. The cells
263 were then washed with FACS buffer and centrifuged at 400 g for 15 min.

264 Next, the cells were resuspended in 1 mL FACS buffer and incubated with the following
265 antibodies for 1 hr on a rotating mixer at 4 °C: CD34-eFluor 660 (1:66), α7-integrin-PE (1:500),
266 biotinylated CD31 (1:200), CD11b (1:200), Ly6A/E (1:200), and CD45 (1:500). The cells were
267 then washed with FACS buffer, centrifuged at 400 g for 15 min, and resuspended in 1 mL FACS
268 buffer. Streptavidin-PE-Cy7 (1:200) was added to the cell suspension, which was then placed on
269 a rotating mixer at 4 °C for 30 min. The cells were then washed with FACS buffer a final time,
270 centrifuged for 15 min at 400 g, and resuspended in 1 mL FACS buffer. Finally, propidium iodide
271 (1:1000) was added to the cells, and MuSCs were enriched by FACS using the following gating
272 strategy: $CD34^+/ITGA7^+/CD45^-/CD31^-/CD11b^-/Ly6A^-/PI^-$.

273 The other method to isolate murine MuSCs from the collective mouse hindlimb muscles
274 was to use Magnetic-Activated Cell Sorting (MACS) based on the vendor protocols (Miltenyi)
275 with adaptations that we found to improve MuSC enrichment. Briefly, the mouse skeletal muscle
276 tissue was processed exactly as described for FACS isolation of MuSCs up to the red blood cell
277 lysis step. After red blood cell lysis, the remaining cells were centrifuged at 400 g for 15 min. The

278 cell pellet was resuspended in 80 µL of FACS buffer and 20 µL of the Satellite Cell Isolation Kit
279 (Miltenyi Biotec, #130-104-268). The cells were incubated for 15 min at 4 °C, after which they
280 were passed through a MACS LS column (Miltenyi Biotec, #130-042-401) mounted on a
281 QuadroMACS separator (Miltenyi Biotec, #130-091-051), and the flowthrough was collected. The
282 column was washed twice with 1 mL FACS buffer, and this wash eluate was combined with the
283 flowthrough of the cells, which was then centrifuged for 5 min at 400 g. The steps of labeling,
284 magnetic depletion and collection of the flowthrough were repeated one more time with a fresh
285 MACS LS column, to maximize the removal of non-MuSC cells. The flowthrough was centrifuged
286 at 400 g for 5 min and resuspended in 80 µL of FACS buffer. 20 µL of anti-integrin α-7 microbeads
287 (Miltenyi Biotec, #130-104-261) was added to the cell suspension and then incubated at 4 °C for
288 15 min, after which the mixture was passed through a fresh MACS LS column mounted on a
289 QuadroMACS separator, to bind MuSCs to the column. The column was washed 3 times with 1
290 mL FACS buffer, and these eluates were discarded. After the washes, the LS column was removed
291 from the magnetic separator and placed on top of a 15 mL collection tube. To collect MACS
292 isolated MuSCs, 5 mL of FACS buffer was then applied to the LS column, and the magnetically
293 labeled cells (i.e., α-7 integrin$^+$) were flushed from the column into the collection tube using the
294 plunger.
295
296 **MACS- and FACS-based Pax7$^+$ cell enrichment purity assessment**
297 To compare the purity of MuSCs isolated using FACS as compared to MACS, Pax7-nGFP mice
298 were humanely euthanized, and their muscles were processed up to the point of incubation in 1
299 mL of red blood cell lysis buffer. After lysis, 10 mL of FACS buffer was added to the cell
300 suspension, which was then evenly split into two 15 mL conical tubes. The tubes were each
301 centrifuged at 400 g for 15 min. One of the tubes was processed based on the MACS isolation
302 protocol, and the other was processed based on the FACS isolation protocol. The cells prepared
303 by each method were then analyzed, using a FACS-Aria machine, with a pressure of 20Psi (low
304 pressure) and 100 µm nozzle diameter, to determine the purity of the isolated cells, which was
305 reported as the % total GFP$^+$ (i.e., Pax7$^+$) cells contained in each sample. Supplementary Figure
306 3 experiments that were conducted to determine the % total GFP$^+$ cells enriched using a variety of
307 optimisations in the MACS protocol were analyzed using the BD Accuri™ C6 Plus Flow
308 Cytometer.

309

310 **Mini-MEndR assay**

311 To conduct mini-MEndR assays, mini-myotube templates were fabricated and then cultured in
312 MEndR DM for a period of 5 days, as described above. Towards the end of differentiation day 6,
313 prospectively isolated MuSCs were resuspended in MuSC GM (Table 2) at a concentration of
314 212,500 cells/mL. Mini-myotube templates were then carefully removed from the 96-well plate
315 using a sterile tweezer and gently placed, with their inverted side up, into the cavities of a sterile
316 custom polydimethylsiloxane (PDMS) block. The PDMS block was placed within an ethanol-
317 sterilized plastic container with a moist paper towel on the bottom to create a humidified chamber.
318 4 μL of resuspended MuSC solution (i.e., 850 cells per tissue) was dispensed onto the tissue
319 surface, and evenly spread using a sterile cell spreader. The plastic container was then sealed with
320 a tight-fitting lid and the stem cell laden myotube templates (i.e., mini-MEndR tissues) were then
321 incubated for 1 hour at 37 °C, to allow the stem cells to incorporate into the mini-myotube
322 template. Following the incubation, tissues were carefully transferred back into their respective
323 96-well plate positions containing MEndR DM supplemented with 5 ng/mL rh-FGF2, and either
324 p38α/β MAPKi or DMSO carrier control (Table 4). The media, containing MEndR DM, FGF2
325 and drug treatments, was completely replaced every other day over the next 5 days. For the
326 remaining duration of the assay, tissues were cultured in MEndR DM, and half of the media was
327 replaced every other day.

328

329 **Statistical Analysis**

330 A minimum of three biological replicates (N) were conducted with multiple technical replicates
331 (n) for most experiments as detailed in Table 5. Statistical analysis was performed using GraphPad
332 Prism 8.0 software. For comparison of two variables, statistical differences were determined by
333 unpaired Student's t-test or unpaired t-test with Welch's correction. For data with more than two
334 variables compared, a one-way ANOVA followed by Tukey's multiple comparison test was
335 utilized (Table 5). All values are expressed as mean ± standard error of the mean (SEM).
336 Significance was defined as $p \leq 0.05$.

337

338 **Results**

339 **Selection of a commercially available cell source for myotube template fabrication**

340 As a first step in establishing a workflow that removed bottlenecks in manufacturing observed in
341 the original MEndR protocols, we set out to select a commercially available primary human
342 myoblast cell line to remove the logistical challenges associated with isolating cells from fresh
343 patient tissue samples. To do this, we differentiated three commercially available primary human
344 myoblast cell lines (Table 1) in 2D culture and compared them across a battery of metrics to select
345 lines for our study that were maximized for differentiation potential and we expected would be
346 minimized for $Pax7^+$ "reserve cell"-mediated self-repair[10,14]. Specifically, we plated primary
347 myoblasts and cultured them for 1 day under growth media (GM) conditions. We then transitioned
348 the cultures to differentiation media (DM), and on the 9th day of differentiation, we fixed the
349 cultures for analysis (Figure 1A). All three cell lines formed multinucleated structures that were
350 immunoreactive for the contractile apparatus protein, sarcomeric α-actinin (SAA; Figure 1B). The
351 18M cell line produced SAA^+ structures that covered a greater proportion of the culture surface
352 area as compared to the other two lines (Figure 1C). We found that all three cell lines performed
353 equivalently with regards to myotube nuclear accretion upon evaluating the proportion of nuclei
354 that contributed to SAA^+ structures (Figure 1D). These data, coupled with visual inspection of the
355 SAA staining (Figure 1B), in turn suggested that the 18M cell line likely produces myotubes of
356 greater diameter than those produced by the other two lines. We found that both the 18F and 19F
357 cell lines had a greater proportion of mononucleated $Pax7^+$ 'reserve cells'[14] present in myotube
358 cultures when compared to the 18M line (Figure 1E). Finally, we confirmed that the cell lines were
359 competent to produce myotubes when resuspended in a 3D fibrin-based hydrogel and cultured in
360 a cellulose scaffold using the original myotube template manufacturing protocol (Figure 1F-H). In
361 all cases, we observed the formation of myotubes structures and similar levels of SAA-coverage
362 within the scaffold (Figure 1G-H). Since our prior studies suggested that excessive reserve cell
363 content can mask the regenerative influence of muscle stem cells added to the assay[10], we elected
364 to move forward with the 18M and 19F lines and abandon the 18F line for this study.
365

366 **Cellulose scaffolds pre-adsorbed with thrombin to allow scalable manufacturing**

367 Having selected commercial cell lines, we set out to establish a workflow for production of
368 myotube templates in a manner that mitigated time-sensitive steps in the original fabrication
369 protocol that we have observed prove challenging for new users that want to adopt the MEndR
370 platform. In the original protocol, myogenic progenitors were resuspended within a fibrinogen /

371 thrombin / Geltrex™ based hydrogel precursor solution, which was subsequently manually
372 distributed over the cellulose scaffold to evenly spread the hydrogel suspensions and encourage
373 infiltration into the scaffold pores prior to hydrogel gelation[10]. A fibrin clot (i.e., hydrogel) forms
374 rapidly upon combining the fibrinogen with thrombin, allowing only a short window of time to
375 resuspend the myogenic progenitors within the solution, dispense the gel-cell solution onto the
376 scaffold, and infiltrate into the cellulose pores. When fabricating only a small (<24) number of
377 scaffolds, this time window is a minimal problem. However, we were concerned that when
378 fabricating 96-scaffolds, this short time window would present a significant challenge. To
379 decouple the hydrogel mixing and gelation steps, we assessed if we could adsorb thrombin (which
380 initiates fibrin gelation), to the cellulose scaffold (Figure 2A). We reasoned that using this
381 approach the myogenic progenitor / fibrinogen / Geltrex™ solution would polymerize in situ only
382 upon making contact with the thrombin-adsorbed cellulose scaffold. We first wanted to confirm
383 that pre-adsorbing fibrin on the scaffold resulted in hydrogel gelation upon infiltration into the
384 scaffold. To this end, we mixed fluorescent beads into the fibrinogen / thrombin / Geltrex™
385 hydrogel precursor solution, infiltrated the solution into the pre-adsorbed scaffold and allowed
386 gelation, imaged the beads, washed vigorously to rinse out any unpolymerized hydrogel (and
387 beads), and then re-imaged the remaining beads to allow us to quantify bead loss due to the
388 washing step (Figure 2A-C). As expected, when no thrombin was present, bead loss occurred upon
389 washing the scaffolds. In conditions where thrombin was directly mixed into the pre-cursor
390 solution, or pre-adsorbed onto the cellulose scaffold, minimal bead loss was observed (Figure 2B-
391 C).
392 When we used this pre-adsorption protocol with myoblasts rather than beads, within one
393 week of culture, we observed thin sheets of multinucleated myotubes form across two cell lines
394 tested (Figure 2D-E). Further, the proportion of 3D tissues covered by SAA^+ myotubes in myotube
395 templates formed using pre-adsorption of thrombin to the scaffold was similar to those formed
396 when thrombin was directly mixed in (Figure 2E-F). We therefore conclude that the pre-adsorption
397 of the thrombin in the cellulose scaffold enabled robust manufacturing of muscle templates that
398 differentiated as expected.
399
400 **Fabrication of myotube templates within a 96-well footprint**

401 We next set out to manufacture MEndR tissues compatible with a 96-well plate footprint. To
402 miniaturize myotube templates from the original 24-well rectangular format[10], we cut sheets of
403 cellulose teabag paper into circular discs using a 5 mm circular biopsy punch (Figure 3A). The
404 circular cellulose scaffolds were autoclaved and then placed into pluronic acid treated wells of a
405 96-well plate using anti-static tweezers. The pluronic acid treatment discouraged myoblast
406 migration or attachment beyond the boundary of the scaffold (Supplementary Figure 1). For both
407 of the myoblast cell lines, we observed formation of multinucleated myotubes by day 7 of
408 differentiation and similar levels of SAA tissue coverage at days 10 and 14 of culture, at which
409 point, we concluded the experiment (Figure 3B-D). SAA tissue coverage at day 7 in the
410 miniaturized format (Figure 3C-D) was similar to that observed in the large format at day 8 for
411 both cell lines (Figure 1H versus Figure 3C and D). Importantly, we found that, in general, three
412 rounds of practice seeding the 96-well format myotube templates using the optimized protocol was
413 sufficient for new users to master the method (Supplementary Figure 2). We therefore concluded
414 that myotube templates could be generated in this smaller dimension format and that new users
415 with myoblast cell culture experience can quickly become proficient with the method.
416
417 **Miniaturized myotube templates possess limited self-repair capacity**
418 Having miniaturized our myotube template platform into a 96-well format, we next set out to
419 demonstrate that our miniaturized platform supported the stem cell mediated repair workflow.
420 Specifically, we wanted to confirm that the miniaturized myotube templates were susceptible to
421 damage induced by cardiotoxin, a snake venom toxin commonly used to induce muscle damage in
422 mouse studies[15]. To do this, on day 7 of mini-myotube template culture, we introduced cardiotoxin
423 to the culture media (Figure 4A). Mini-myotube templates were fixed 24 hrs after the initial
424 cardiotoxin exposure and immunostained to visualize and quantify the resulting SAA^+ myotube
425 structures (Figure 4A-D). We observed a 21.31% +/- 4.37% and 24.12% +/- 5.24% decrease in
426 SAA immunoreactivity one day after cardiotoxin treatment in myotube templates generated from
427 the 18M and 19F myoblast lines, respectively, consistent with prior results obtained using the
428 larger myotube template format (Figure 4C-D)[10].
429 We next analyzed the mini-myotube templates 10 days after cardiotoxin exposure, to
430 determine whether $Pax7^+$ reserve cell activity alone regenerated the injured myotube templates
431 (Figure 5). Similar to the larger myotube template format[10], we found that the SAA content failed

432 to return to levels observed in the uninjured control (Figures 5B-D, DMSO CTX(-) vs CTX (+)).
433 As expected, when templates were treated with an inhibitor of p38 α/β MAP kinase (p38i), a
434 treatment known to expand both muscle stem and progenitor cells[8], we observed that SAA content
435 was able to return to levels matching the uninjured control (Figure 5B-D). By contrast, treatment
436 with an epidermal growth factor receptor inhibitor (EGFRi) failed to stimulate reserve cell-
437 mediated myotube template repair, as measured by SAA coverage (Figure 5B-D). Together, these
438 results confirmed that the mini-myotube templates were receptive to injury, and had limited self-
439 repair capacity, allowing for enhancement by introducing freshly isolated MuSCs.
440

441 **A MACS-based MuSC enrichment strategy supports MEndR assay scale-up**

442 We next set out to demonstrate that muscle stem cell mediated skeletal muscle tissue repair occurs
443 in the miniaturized myotube template format. We previously showed that freshly FACS-sorted
444 MuSCs introduced to injured myotube templates contribute to the process of tissue repair by
445 producing new myotubes[10]. For these studies, we prospectively isolated MuSCs from
446 enzymatically digested murine skeletal muscle tissue using a magnetic-activated cell sorting
447 (MACS) strategy (Supplementary Figure 3), which we first confirmed to produce similar results
448 as compared to MuSCs isolated using a traditional fluorescence activated cell sorting (FACS)
449 protocol (Supplementary Figure 4). For this comparison, we harvested hindlimb skeletal muscle
450 tissue from humanely euthanized Pax7-nGFP transgenic reporter mice (Supplementary Figure 3)
451 or those ubiquitously expressing yellow fluorescent protein (YFP; Supplementary Figure 4) and
452 subjected it to standard mechanical dissociation and enzymatic digestion protocols to produce a
453 single cell suspension. The cell suspension was split equally, processed, and sorted
454 (Supplementary Figure 3A) using either a FACS (Supplementary Figure 3B-C) or MACS-based
455 protocol (Supplementary Figure 3C-D). The cell populations harvested from Pax7-nGFP animals
456 were characterized immediately after enrichment using flow cytometry (Supplementary Figure
457 3C). We found that 97.87% +/- 2.24% of events from FACS-enriched events were GFP^+, whereas
458 91.70% +/- 0.97% of events were GFP^+ following a modified MACS enrichment strategy
459 (Supplementary Figure 3C-D). We speculated that the greater proportion of GFP-negative cells
460 within the MACS-enriched cell population could be owed to integrin α-7^+ contaminating cell
461 types[16], or that it may be an artifact of magnetic-enrichment protocols which are less effective than
462 FACS at removing cellular debris. In prior studies, we plated the FACS and MACS-enriched cell

463 populations in culture and then 12 hrs later, enumerated the viable GFP positive and negative cells
464 in each well[17]. This uncovered a dramatic loss of the GFP-negative population from the MACS-
465 enriched cell population, resulting in an enrichment for GFP-positive cells that matched values
466 obtained using FACS-enrichment. Anecdotally, we have found that increased experience using the
467 MACS method correlated with a consistently higher proportion of GFP^+ cells in the populations
468 enriched from Pax7-nGFP transgenic animals (data not shown). It is also worth noting that in our
469 experience MACS-based enrichment consistently offered higher cell yields when compared to the
470 FACS-based strategy (data not shown). Together this data suggested that MACS was a feasible
471 and convenient method for sorting MuSCs from mouse hindlimb skeletal muscle tissue for our
472 scaled MEndR assay.
473
474 **Miniaturized format supports muscle endogenous repair (mini-MEndR) assays**
475 We next wanted to confirm that our miniaturized myotube template system, seeded with MuSCs,
476 could replicate key results observed using the original MEndR assay which successfully identified
477 and recapitulated outcomes of known stimulators of murine muscle stem cell mediated muscle
478 tissue repair[10]. We generated myotube templates, and then on day 6 of differentiation we
479 introduced MACS enriched MuSCs from YFP-transgenic animals. 12 hr after MuSC engraftment,
480 co-cultures were then exposed to cardiotoxin to injure the myotube templates, after which we
481 introduced to the culture media p38 α/β MAPK inhibitor (p38i), a known modulator of stem cell
482 skeletal mediated repair, or DMSO carrier control. At 7 or 10 days post-injury (DPI), the tissues
483 were fixed and immunostained to evaluate the donor-derived contributions to muscle tissue repair
484 (Figure 6A-B). Consistent with our results in the large MEndR format, we observed increased
485 donor derived myotube formation in tissues treated with p38i, suggesting enhanced stem cell
486 mediated repair that was apparent at 10 DPI (Figure 6C-D). This effect was observed when MuSCs
487 were introduced to myotube templates generated from both the 18M and 19F primary myoblasts
488 (Figure 6C-D). Further, MuSCs prospectively isolated using the MACS-enrichment method
489 performed in a functionally equivalent manner by this metric when compared against those sorted
490 using a classic FACS-based method (Supplementary Figure 4). The effect of p38i on donor
491 myotube production was detectable statistically by 7 DPI, and was not significantly different from
492 the results obtained at 10 DPI. This observation suggests that a shortened timeline to assess stem

493 cell-mediated muscle production using the mini-MEndR assay is feasible, benefiting future
494 screening applications.

495 We next assessed another key read-out of stem cell mediated skeletal muscle repair, niche
496 repopulation, which we have shown is captured in the original MEndR format[10]. For these studies,
497 we repeated the protocol described above, using instead MuSCs isolated from Pax7-nGFP
498 transgenic reporter animals (Figure 7A). On day 7 post-injury, when tissue repair was complete,
499 we observed a population of mononucleated Pax7$^+$ donor-derived (GFP; Figure 7B), which we
500 previously showed had reversibly exited cell cycle[10]. Further, and in line with results obtained in
501 the original MEndR platform, we observed a ~3-fold increase in these donor-derived Pax7$^+$ cells
502 in response to p38i treatment (Figure7C-D). The MEndR and mini-MEndR assays were designed
503 as a mixed species cell 'competition' assay in part to enable multiplexed analyses of human and
504 mouse Pax7$^+$ populations within the same assay. The mouse Pax7$^+$ cell population is isolated from
505 a transgenic animal and therefore easily distinguished from the unlabeled Pax7$^+$ 'reserve cells' that
506 exist within the primary human myoblast population, which is used to fabricate the myotube
507 template. Thus, enumerating the mononucleated Pax7 immunoreactive cells present in the
508 myotube template at the end-point of a mini-MEndR assay, while tracking whether they are GFP
509 labeled (mouse) or unlabeled (human) enables a cursory assessment of species specific Pax7$^+$ cell
510 responses. Consistently, when we enumerated the Pax7$^+$ reserve cell abundance at the assay end-
511 point, treatment with the p38i produced an increase in the incidence of mononucleated Pax7$^+$
512 reserve cells (Figure 7E-F).

513 Together this data suggested that the miniaturized muscle endogenous repair assay (mini-
514 MEndR) replicated all of the stem cell functional metrics previously reported in the original large
515 format MEndR assay.

516

517 **Discussion**

518 In this paper we set out to miniaturize and improve the manufacturing workflow of our
519 previously reported skeletal muscle stem cell mediated repair assay, known as MEndR[10] to
520 enable wider adoption of this powerful assay to identify novel molecular targets that promote
521 muscle regeneration. We addressed three critical bottlenecks in the workflow of the original
522 MEndR assay, that have up until now limited its capacity to assess molecular targets at a
523 practically useful scale. Firstly, we demonstrate use of primary human myoblasts from a

524 commercial source to generate the myotube template to reduce myotube template variation
525 associated with the use of different muscle biopsy donors. Second, we developed a method to
526 integrate the hydrogel crosslinker into the scaffold to trigger in situ gelation to counter the rapid
527 gelation properties of the fibrin hydrogel used to manufacture the myotube template, which had
528 limited the number of myotube templates that can be robustly manufactured using one batch of
529 myoblast-hydrogel suspension. Third, we validate the use of an alternative to FACS for sorting
530 skeletal muscle stem cells from digested skeletal muscle which overcomes limits on the number
531 of wells that can be assessed in parallel using freshly isolated adult stem cells. Further, we
532 miniatured the format of the assay ~6-fold to reduce both the number of template cells and added
533 stem cells required per well to perform the assay.

534 The use of cross-linker adsorption to the paper scaffold to enable in situ hydrogel gelation
535 during tissue manufacturing was particularly critical to able scalable manufacturing of the
536 myotube template due to the rapid gelation of fibrin upon addition of the thrombin crosslinker to
537 the bulk hydrogel solution containing the myoblasts. We anticipate this innovation could enable
538 the manufacturing of myotube templates using robotic liquid handling in the future to support
539 tissue manufacturing for large scale screening efforts. Indeed this strategy could potentially be
540 utilized to generate tissues for other applications that use two component hydrogels in which gel
541 crosslinking is initiated by the addition of an external crosslinking component as opposed to
542 simply a temperature change alone. Interestingly, we observed that the use of thrombin pre-
543 adsorption dramatically reduced the number of attempts required to master the mini-MEndR
544 seeding protocol, which suggests that pre-mature hydrogel gelation could be a key source of
545 inter-well variation in other paper-based systems[11,18].

546 While this work successful increased the throughput capacity of our MEndR assay to
547 enable potential screening of drug candidates at a 96-well plate scale, it is important to note some
548 remaining limitations of the mini-MEndR assay. We note that removal of the myotube template
549 from each well to integrate the muscle stem cells remains a rate limiting step in our work flow.
550 However, this step does not significantly impact usability at a 96-well plate throughput. A 96-
551 well throughput is appropriate for assessing 10s to 100s of targets. This manual removal step,
552 however would limit use of robots in fully automating our assay. If a larger scale screening
553 capacity is desirable in the future, the MEndR assay could be further integrated with the SPOT

554 platform[18], reported by our group, which we recently demonstrated is compatible with robotic
555 liquid handler to enable massive increases in scale[19].
556 Given that the myotube template contains a population of Pax7$^+$ reserve cells that have
557 the potential to contribute to myotube template repair, even in the absence of adding a MuSC
558 population, means that readouts of mini-MEndR SAA-coverage alone are not able to distinguish
559 between drugs that target this reserve cell population versus those that target the MuSC
560 population specifically. Thus, it is important for MuSCs that are added to mini-MEndR
561 experiments to be fluorescently labeled to disentangle MuSC and template reserve cell
562 regenerative activities. An advantage of conducting mixed species mini-MEndR experiments is
563 the ability to track the influence of treatments on both human Pax7$^+$ reserve cell and mouse
564 MuSC self-renewal and differentiation within the same experiment. The user has complete
565 control over MuSC content in each experiment, but limited control over the drift in Pax7$^+$ reserve
566 cell content. Further, there is ongoing debate with regards to drawing conclusions about human
567 MuSC biology based solely on human Pax7$^+$ reserve cell studies. For example, EGFRi treatment
568 induced different effects on mouse MuSCs as compared to human Pax7$^+$ reserve cells based
569 upon our experiments, and whether this reflects an influence of species or is a MuSC vs reserve
570 cell difference has yet to be determined. Thus, downstream studies to evaluate the effects of
571 'hits' on bonefide human MuSCs are to be expected, and adaptions of the assay to integrate
572 MuSC freshly enriched from human muscle biopsies are underway. The capacity to conduct
573 follow up experiments at a higher scale in combination with the compatibility of mini-MEndR
574 tissues to be imaged semi-automatically with high-content imaging systems will serve to
575 facilitate follow up dose response and mechanistic studies of molecular targets identified in the
576 initial screen.
577
578 **Conclusions**
579 Identification of drugs to boost the capacity of MuSCs to drive skeletal muscle endogenous repair
580 is an exciting approach to address various conditions that lead to impaired skeletal muscle
581 regeneration, such as aging or DMD. The MEndR assay provides a powerful functional assay "in
582 a dish" with the potential to identify molecular targets that enhance human skeletal muscle
583 endogenous repair. Here we adapted the original MEndR manufacturing workflow to enable the
584 robust manufacturing of a 96-well plate "mini-MEndR" platform. Further we validated that this

585 miniaturized platform recapitulates the known endogenous repair readouts captured in the original
586 larger MEndR format. The mini-MEndR platform has the potential to enable the identification of
587 novel molecular targets to modulate stem-cell mediated skeletal muscle repair and to facilitate an
588 exploration of their cellular and molecular mechanism(s) of action.
589

590 **Acknowledgements**

591 N.G., S.D., and B.X. contributed equally to this work. S.R., and E.J. contributed equally to this
592 work. BioRender was utilized to produce schemata elements. This project was funded by a Canada
593 First Research Excellence Fund "Medicine by Design (MbD)" grant to P.M.G. and A.P.M.
594 (MbDC2-2019-02), a Natural Sciences and Engineering Research Council of Canada (NSERC)
595 Idea to Innovation grant awarded to A.P.M. and P.M.G. (I2IPJ 549768-20), a University of
596 Toronto Connaught Fund awarded to A.P.M. and P.M.G., a Canada Research Chair in Endogenous
597 Repair award to P.M.G. (#950-231201), Stem Cell Network grant to P.M.G. (#FY20/DRP-1),
598 Ontario Institute for Regenerative Medicine grant to P.M.G. (#2018-0510), CGS-D Awards to B.X.
599 and E.J., a CGS-M Award to S.R., an NSERC CREATE TOeP scholarship to S.D., Ontario
600 Graduate Scholarships to B.X., S.R., and E.J. and a Norman F. Moody Award to B.X.
601

602 **Author contributions**

603 N.G., S.D., B.X., S.R., E.J., J.P., and A.F. designed and performed research, analyzed data, and
604 prepared figures. A.P.M., P.M.G., and S.D. conceived of the project and supervised the research.
605 All authors contributed to data interpretation. A.P.M., P.M.G., N.G., B.X., and S.R. wrote the
606 manuscript. All authors reviewed and approved the manuscript.
607

608 **Conflict of Interest**

609 The authors have no competing interests, or other interests that might be perceived to influence
610 the results and/or discussion reported in this paper.
611

612 **Data and Materials Availability Statement**

613 The datasets generated during and analyzed in this study are available from the corresponding
614 author on reasonable request.
615

616 **References**

617 1. Brunet, A., Goodell, M. A. & Rando, T. A. Ageing and rejuvenation of tissue stem cells and
618 their niches. *Nat. Rev. Mol. Cell Biol.* **24**, 45–62 (2023).
619 2. Dumont, N. A. *et al.* Dystrophin expression in muscle stem cells regulates their polarity and
620 asymmetric division. *Nat. Med.* **21**, 1455–1463 (2015).
621 3. Wang, Y. X. *et al.* EGFR-Aurka Signaling Rescues Polarity and Regeneration Defects in
622 Dystrophin-Deficient Muscle Stem Cells by Increasing Asymmetric Divisions. *Cell Stem*
623 *Cell* **24**, 419—-432.e6 (2019).
624 4. Rozo, M., Li, L. & Fan, C. M. Targeting β1-integrin signaling enhances regeneration in aged
625 and dystrophic muscle in mice. *Nat. Med.* **22**, 889–896 (2016).
626 5. Porpiglia, E. *et al.* Elevated CD47 is a hallmark of dysfunctional aged muscle stem cells that
627 can be targeted to augment regeneration. *Cell Stem Cell* **29**, 1653-1668.e8 (2022).
628 6. Benjamin, D. I. *et al.* Fasting induces a highly resilient deep quiescent state in muscle stem
629 cells via ketone body signaling. *Cell Metab.* **34**, 902-918.e6 (2022).
630 7. Gilbert, P. M. *et al.* Substrate elasticity regulates skeletal muscle stem cell self-renewal in
631 culture. *Science* **329**, 1078–1081 (2010).
632 8. Cosgrove, B. D. *et al.* Rejuvenation of the muscle stem cell population restores strength to
633 injured aged muscles. *Nat. Med.* **20**, 255–264 (2014).
634 9. Sacco, A., Doyonnas, R., Kraft, P., Vitorovic, S. & Blau, H. M. Self-renewal and expansion
635 of single transplanted muscle stem cells. *Nature* **456**, 502–506 (2008).
636 10. Davoudi, S. *et al.* MEndR: An in vitro functional assay to predict in vivo muscle stem cell-
637 mediated repair. *Adv. Funct. Mater.* (2021).

638 11. Rodenhizer, D., Dean, T., Xu, B., Cojocari, D. & McGuigan, A. P. A three-dimensional
639 engineered heterogeneous tumor model for assessing cellular environment and response. *Nat.*
640 *Protoc.* **13**, 1917–1957 (2018).
641 12. Sambasivan, R. *et al.* Distinct regulatory cascades govern extraocular and pharyngeal arch
642 muscle progenitor cell fates. *Dev Cell* **16**, 810–821 (2009).
643 13. Davoudi, S. *et al.* Muscle stem cell intramuscular delivery within hyaluronan
644 methylcellulose improves engraftment efficiency and dispersion. *Biomaterials* **173**, 34–46
645 (2018).
646 14. Laumonier, T., Bermont, F., Hoffmeyer, P., Kindler, V. & Menetrey, J. Human myogenic
647 reserve cells are quiescent stem cells that contribute to muscle regeneration after
648 intramuscular transplantation in immunodeficient mice. *Sci. Rep.* **7**, 3462 (2017).
649 15. Hardy, D. *et al.* Comparative Study of Injury Models for Studying Muscle Regeneration in
650 Mice. *PloS One* **11**, e0147198 (2016).
651 16. Giordani, L. *et al.* High-Dimensional Single-Cell Cartography Reveals Novel Skeletal
652 Muscle-Resident Cell Populations. *Mol. Cell* **74**, 609-621.e6 (2019).
653 17. Jacques, E. *et al.* The mini-IDLE 3D biomimetic culture assay enables interrogation of
654 mechanisms governing muscle stem cell quiescence and niche repopulation. *eLife* **11**,
655 e81738 (2022).
656 18. Li, N. T. *et al.* An off-the-shelf multi-well scaffold-supported platform for tumour organoid-
657 based tissues. *Biomaterials* **291**, 121883 (2022).
658 19. Cao, R. *et al.* An automation workflow for high-throughput manufacturing and analysis of
659 scaffold-supported 3D tissue arrays.

660 http://biorxiv.org/lookup/doi/10.1101/2022.08.20.504600 (2022)

661 doi:10.1101/2022.08.20.504600.

662

663 **Figure Legends**

664 **Figure 1. Characterization of commercially available human pMB lines. (A)** Experimental
665 timeline for the 2D differentiation of the human primary myoblasts. **(B)** Representative 10X
666 confocal images of the three commercially available human myoblasts immunostained for
667 sarcomeric α-actinin (SAA; magenta) and counterstained for DRAQ5 (grey) on day 9 of
668 differentiation in 2D culture. Scale bar, 500 µm. **(C-E)** Bar graphs quantifying SAA coverage **(C**),
669 average nuclear fusion index **(D)**, and ratio of $Pax7^+$ reserve cells amongst the mononuclear cells
670 **(E)** in 2D culture on day 9 differentiation comparing the three cell lines. Graphs display mean ±
671 s.e.m., one-way ANOVA with Tukey post-test. ** $p < 0.01$, *** $p < 0.001$, **** $p < 0.0001$, ns. -
672 no significance. n=3 wells from N=1 experiment per cell line. **(F)** Schematic of the 24-well
673 myotube template derivation workflow. **(G)** Representative confocal images of SAA (magenta)
674 immunostaining in myotube templates at day 8 of differentiation that were generated using the
675 18M, 18F and 19F cell lines. Scale bar, 500 µm. **(H)** Bar graph quantification of myotube template
676 SAA coverage at day 8 of differentiation. Graphs display mean ± s.e.m., one-way ANOVA with
677 Tukey post-test, ns. – no significance. n=2 tissues from N =1 experiment per cell line.

678

679 **Figure 2. Preabsorbing thrombin in paper scaffolds to facilitate myotube template seeding.**
680 **(A)** Schematic of the bead assay workflow. Cellulose scaffolds were pre-adsorbed with thrombin
681 and seeded with fluorescent beads diluted 10 times in ECM master mix. The beads were imaged
682 before and after washing to quantify bead retention. **(B)** Representative confocal images of bead
683 assay paper scaffolds before and after washing. Scale bar, 500 µm. **(C)** Quantification of the
684 number of beads before washing (black) and after washing (grey) for fluorescent beads seeded on
685 paper scaffolds without thrombin, with 0.8 U/ml thrombin mixed-in, or with 0.8 U/ml thrombin
686 pre-adsorption. Graphs display mean ± s.e.m., two-way ANOVA followed by Sidak's multiple
687 comparisons test *** $p < 0.001$, N=2, n=8. **(D)** Experimental workflow for comparing thrombin
688 mixed-in (left) to pre-adsorption (right) methods on myotube template formation. **(E)**
689 Representative confocal images of myotube template stained for phalloidin (magenta) after 7 days

690 of differentiation. Scale bar, 500 µm. **(F)** Quantification of phalloidin coverage for thrombin
691 mixed-in vs pre-adsorption methods. ns. = no significance. n=11-24 tissues from N=3-4
692 independent experiments.
693
694 **Figure 3**. **Mini-myotube template derivation. (A)** Schematic of the mini-myotube template
695 derivation workflow. Cellulose scaffolds were pre-adsorbed with thrombin and seeded with human
696 pMBs mixed in an ECM mixture containing DMEM, fibrinogen and Geltrex^{TM}. **(B)** Representative
697 confocal images of SAA (magenta) immunostaining for mini-myotube templates generated with
698 the 18M and 19F cell lines and analyzed on days 7, 10, and 14 of differentiation. Scale bar, 500
699 µm. **(C, D)** Quantification of SAA coverage in mini-myotube templates generated with the 18M
700 **(C)** and 19F **(D)** cell lines on days 7, 10, and 14 of differentiation. Graphs display mean ± s.e.m.
701 one-way ANOVA with Tukey post-test. * $p < 0.05$, ** $p < 0.01$ ns. = no significance. n = 6-10
702 tissues from N = 3-4 independent experiments per cell line.
703
704 **Figure 4. Myotoxin-induced mini-myotube templates injury. (A)** Schematic of the template
705 injury workflow. Mini-myotube templates are incubated in MEndR differentiation media
706 containing 0.5 µm cardiotoxin (CTX) for 4 hr at 37 °C on an orbital shaker. **(B)** Representative
707 confocal images of uninjured (left; (-)) and injured (right; (+)) mini-myotube templates generated
708 with the 18M (top) or 19F (bottom) cell lines (SAA; magenta) at 1 DPI. Scale bar, 500 µm. **(C,**
709 **D)** Quantification of SAA tissue coverage in uninjured and injured mini-myotube templates
710 generated with 18M **(B)** or 19F **(C)** cell lines at 1 DPI. Graphs display mean ± s.e.m. Unpaired
711 student's t-test, **** $p < 0.0001$. n =11-20 tissues from N=5-6 independent experiments per cell
712 line.
713
714 **Figure 5. p38α/β MAPKi, but not EGFRi, induces mini-myotube template self-repair. (A)**
715 Experimental timeline to study mini-myotube template self-repair capacity. **(B)** Representative
716 confocal images of uninjured (CTX(-)) and injured (CTX(+)) myotube templates generated with
717 18M (top) or 19F (bottom) cell lines in response to treatment with p38α/β MAPK inhibitor (p38i),
718 epidermal growth factor inhibitor (EGFRi) or DMSO carrier control at 10 DPI. Scale bar, 500 µm.
719 **(C, D)** Quantification of SAA coverage in uninjured and injured myotube templates generated with
720 18M **(C)** or 19F **(D)**. Graphs display mean ± s.e.m. one-way ANOVA with Tukey post-test, *

721 p<0.05, ** p < 0.01, *** p < 0.001, **** p < 0.0001. n =10-15 tissues from N=4-5 independent
722 experiments per cell line.
723
724 **Figure 6. p38α/β MAPKi treatment augments MuSC-mediated muscle production in mini-**
725 **MEndR assay. (A)** Schematic of the mini-MEndR assay workflow. MuSCs from YFP transgenic
726 mice are isolated using the adapted magnetic assisted cell sorting (MACS) protocol and then
727 engrafted onto the mini-myotube templates on day 6 of differentiation, followed by drug
728 treatments and cardiotoxin-induced tissue injury. **(B)** Detailed experimental timeline for the mini-
729 MEndR assay workflow. **(C)** Representative confocal images of MuSC-mediated (YFP^+) myotube
730 production in the injured mini-myotube templates produced with 18M (top panel) 19F (bottom
731 panel) in response to treatment with DMSO or p38α/β MAPKi harvested at 7 DPI. Scale bar, 500
732 µm. (**D-E)** Quantification of the MuSC-mediated regeneration (%YFP coverage) in the injured
733 mini-myotube templates generated with 18M **(D)** or 19F **(E)** cell line harvested at 7 DPI or 10 DPI.
734 Graphs display mean± s.e.m; Unpaired two-tailed T-test with Welch's correction was conducted
735 for each condition. * p<0.05, ** p < 0.001, **** p, n=9-12 tissues from N=3-4 independent
736 experiments per cell line.
737
738 **Figure 7. mini-MEndR assay captures response of treatment known to stimulate MuSC self-**
739 **renewal. (A)** Detailed experimental timeline of donor-derived MuSC niche repopulation. **(B)**
740 Representative confocal images of $Pax7^+GFP^+$ donor derived MuSCs in mini-MEndR tissues
741 treated with p38α/β MAPKi at 7 DPI. Tissues are immunostained for Pax7 (grey), GFP (green),
742 and DAPI (cyan). Magenta arrowheads point to the $Pax7^+$ GFP^+ donor MuSCs and yellow
743 arrowheads point to the $Pax7^+$ GFP^- reserve cells derived from the myotube template. Scale bar,
744 50 µm. **(C-F)** Quantification of $Pax7^+$ GFP^+ cells derived from donor MuSCs (**C-D**) or $Pax7^+$ GFP^-
745 reserve cells derived from the myotube template (**E-F**) in mini-MEndR tissues generated with 18M
746 **(C, E)** and 19F **(D, F)** cell lines, following treatment with DMSO or p38α/β MAPKi in the context
747 of injury and analyzed at 7 DPI. Graphs display mean ± s.e.m.; Unpaired two-tailed T-test with
748 Welch's correction. * p < 0.5, *** p < 0.001, **** p < 0.0001. n=6-9 tissues from N=3 independent
749 experiments per cell line.
750
751 **Supplementary Figure Legends**

752 **Supplementary Figure 1. Pluronic acid coating allows for the generation of smooth mini-**
753 **myotube template edges.** Representative confocal images of mini-myotubes generated with (+)
754 and without (-) pluronic acid coating. Tissues are immunostained for sacromeric α-actinin (SAA;
755 magenta). Scale bar, 1 mm.
756
757 **Supplementary Figure 2. Mini-MEndR platform manufacture can be quickly mastered by**
758 **new users. (A)** Representative confocal images of myotube templates generated by the same user
759 at different levels of experience. Tissues were fixed after 7 days of differentiation and stained with
760 phalloidin (magenta). Scale bar, 500 µm. **(B)** Quantification of Phalloidin (User 1) or SAA (User
761 2, 3) tissue coverage attained by three different users who trained from first-time user to expert
762 level as indicated by plateauing coverage and homogeneous mini-myotube templates. Coverage
763 was normalized to the average of each user's three most recent seeding attempts at expert level to
764 account for cell line-to-cell line differences in absolute fiber coverage.
765
766 **Supplementary Figure 3. Gating strategy used for MACS or FACS based MuSCs isolation.**
767 **(A)** Schematic showcasing the workflow of MACS vs FACS MuSC isolation protocols. **(B)** Flow
768 cytometry plots demonstrating gating strategy to enrich MuSCs from Pax7-nGFP transgenic mice
769 using FACS. **(C)** Representative plots of green fluorescent protein $(GFP)^+$ cells present in MuSC
770 preparations derived from Pax7-nGFP tissue samples using FACS (left) as compared to MACS
771 (right)**. (D)** Enumeration of % total GFP^+ cells enriched from Pax7-nGFP tissue samples using a
772 variety of optimisations that include the number of lineage depletion column rounds with or
773 without an integin-α7 column enrichment round performed during the MACS protocol.
774
775 **Supplementary Figure 4. MACS and FACS sorted MuSCs are functionally similar in mini-**
776 **MEndR assays. (A)** Representative confocal images and **(B)** quantification of yellow fluorescent
777 protein (YFP; yellow) immunostaining coverage of 18M mini-MEndR tissues at 10 DPI that were
778 generated with FACS or MACS sorted MuSCs and treated with DMSO. Scale bar, 500 µm. Graphs
779 display mean ± s.e.m.; unpaired two-tailed T-test with Welch's correction, ns = no significance.
780 n=9-10 tissues from N = 3 independent experiments per cell line.
781
782 **Table 1. Human skeletal muscle myoblast donor information**

783

Age	Sex	Ethnicity	Vendor	Catalog #	Tissue of Origin	Additional Information
18	M	Caucasian	Cook MyoSite	SK-1111-P01236-18M	Rectus Abdominus	Active
18	F	Caucasian	Cook MyoSite	SK-1111-P01431-18F	Vastus Lateralis	Healthy, No known medical conditions
19	F	Caucasian	Cook MyoSite	SK-1111-P01358-19F	Vastus Lateralis	N/A

784

785

786 **Table 2. Culture medium and solutions**

787

Media	Composition
Wash Medium	10 % FBS, 90 % DMEM
Human pMB Growth Medium	Ham's F-10 nutrient mix, 20 % Foetal bovine serum FBS, 5 ng/mL rh-FGF2, 1 % Penicillin-Streptomycin
2D Differentiation Media	DMEM, 2 % Horse serum, 10 g/mL insulin (Sigma, #I6634), 1 % Penicillin-Streptomycin
Rat Tail Collagen Solution	0.1 M Acetic Acid, Collagen I Rat Tail Stock solution (Gibco #A1048301), 0.1 M Acetic Acid, Collagen Stock Solution
MuSC Growth Medium	DMEM/F12, 1 % Pen-strep (P/S), 20 % Foetal bovine serum (FBS), 10 % Horse serum (HS), 1 % 2 mM Q (Glutamax), 1 % Insulin-Transferrin-Selenium (ITS), 1 % Non-Essential Amino acids, 1 % 1 mM Sodium Pyruvate, 50 uM (1/1,000) β-mercaptoethanol, 5 ng/ml (1/5,000) Gibco FGF2
MEndR Growth Medium	Ham's F-10 nutrient mix, 20 % FBS, 1.5 mg/mL 6-Aminocaproic Acid (ACA, Sigma, #A2504), 1 % Penicillin-Streptomycin
MEndR Differentiation Medium	DMEM, 2 % Horse serum, 2 mg/mL ACA, 10 g/mL insulin (Sigma, #I6634), 1 % Penicillin-Streptomycin
Fibrinogen Solution	10 mg/mL Fibrinogen (Sigma, #F8630) in NaCl solution (0.9 % wt/vol in ddH2O)
Extracellular Matrix (ECM) Master Mix	40 % DMEM, 40 % Fibrinogen, 20 % Geltrex™

Red Blood Cell Lysis Buffer	H_2O, 0.155 M NH_4Cl, 0.01 M $KHCO_3$, 0.1 mM EDTA
FACS Buffer	PBS, 2.5 % goat serum, 2 mM EDTA
Blocking Solution	PBS, 10 % goat serum, 0.3 % Triton X-100 (BioShop, #TRX777)

788

789 **Table 3. Antibodies and other reagents**

790

Antibody	Host species	Dilution	Manufacturer
Alexafluor® 647 Anti-Human CD56	Mouse	1:20 (FC)	BD, #557711
eFluor® 660 Anti-Mouse CD34	Rat	1:66 (FC)	eBioscience, #50034182
PE Anti-Mouse α7-Integrin	Rat	1:500 (FC)	AbLab, #530010-05
Biotin Anti-Mouse CD31	Rat	1:200 (FC)	BD, #553371
Biotin Anti-Mouse CD45	Rat	1:500 (FC)	BD, #553078
Biotin Anti-Mouse CD11b	Rat	1:200 (FC)	BD, #553309)
Biotin Anti-Mouse Ly-6A/E	Rat	1:200 (FC)	BD, #553334
Propidium Iodide	-	1:1000	Sigma, # P4864
Anti-Sarcomeric α-actinin	Mouse	1:500	Sigma, #A7811
Anti-GFP	Rabbit	1:500 (IF)	ThermoFisher, #A11122
Anti-Pax7	Mouse	1.5:1 (IF)	Iscove
Alexafluor® 488 Anti-Rabbit	Goat	1:500 (IF)	ThermoFisher, #A11008
Alexafluor® 546 Anti-Mouse	Goat	1:500 (IF)	ThermoFisher, #A11003
Alexafluor® 647 Anti-Rat	Goat	1:500 (IF)	ThermoFisher, #A21247
Phalloidin 568	-	1:500 (IF)	Life Technologies, #A12380

Hoechst	-	1:1000 (IF)	ThermoFisher, #H3570
DRAQ5	-	1:1000 (IF)	Cell Signaling Technology, #4084L
DAPI	-	1:1000 (IF)	Roche, #10236276001
Satellite Cell Isolation Kit	Mouse	1:5 (MACS)	Miltenyi Biotec, #130-104-268
Anti-Integrin-α7 Beads	Mouse	1:5 (MACS)	Miltenyi Biotec, #130-104-261
Click-iT™ Plus EdU Cell Proliferation Kit		(EdU, 1 μM)	ThermoFisher, #C10638

791

792 **Table 4. Small molecule information**

Drug name	Target	Working concentration	Manufacturer
SB203580	p38α/β MAPK	10 μM	New England biolabs, #5633
Erlotinib Hydrochloride	Epidermal Growth Factor Receptor (EGF)	5 μM	Sigma Aldrich, #sc-202154
DMSO	-	-	Sigma Aldrich, #D2650

793

794 **Table 5. Statistical tests and analysis**

Figure	Biological experiments (N)	Total tissues/wells per condition (n)	Total images/wells per tissue	Statistical tests
1C	1 per cell line	3	5	Ordinary one-way ANOVA with Tukey's multiple comparison's test
1D	1 per cell line	3	5	Ordinary one-way ANOVA with Tukey's multiple comparison's test
1E	1 per cell line	3	5	Ordinary one-way ANOVA with

				Tukey's multiple comparison's test
1H	1 per cell line	2	3	Ordinary one-way ANOVA with Tukey's multiple comparison's test
2C	2	8	1	Two-way ANOVA with Sidak's multiple comparisons test
2F	Mixed in: 3 Pre-adsorped: 4	Mixed in: 11 Pre-adsorped:24	1	Unpaired two-tailed t-test
3C	3	Day 7: 9 Day 10: 10 Day 14: 10	1	Ordinary one-way ANOVA with Tukey's multiple comparison's test
3D	3	Day 7: 9 Day 10: 8 Day 14: 6	1	Ordinary one-way ANOVA with Tukey's multiple comparison's test
4C	6	CTX (-): 18 CTX (+): 20	1	Unpaired t-test
4D	5	CTX (-): 15 CTX (+): 16	1	Unpaired t-test
5C	5	DMSO CTX (-):15 DMSO CTX (+):15 p38i CTX (+):15 EGFRi CTX (+):15	1	Ordinary one-way ANOVA with Tukey's multiple comparison's test
5D	4	DMSO CTX (-):12 DMSO CTX (+):12 p38i CTX (+):12 EGFRi CTX (+):10	1	Ordinary one-way ANOVA with Tukey's multiple comparison's test
6C	4	DPI7 DMSO: 11 DPI7 p38i:12 DPI10 DMSO:11 DPI10 p38i:10	1	Multiple t-tests with Welch's correction
6D	3	DPI7 DMSO: 9 DPI7 p38i:9	1	Multiple t-tests with Welch's correction

		DPI10 DMSO:8 DPI10 p38i:9		
7C	3	DMSO: 6 p38i: 8	4-7	Unpaired two-tailed T-test with Welch's correction
7D	3	DMSO: 7 P38i: 8	4-7	Unpaired two-tailed T-test with Welch's correction
7E	3	DMSO: 6 p38i: 8	4-7	Unpaired two-tailed T-test with Welch's correction
7F	3	DMSO: 7 P38i: 8	4-7	Unpaired two-tailed T-test
SI 4B	3	FACS: 9 MACS: 10	1	Unpaired two-tailed T-test with Welch's correction

Figure 1

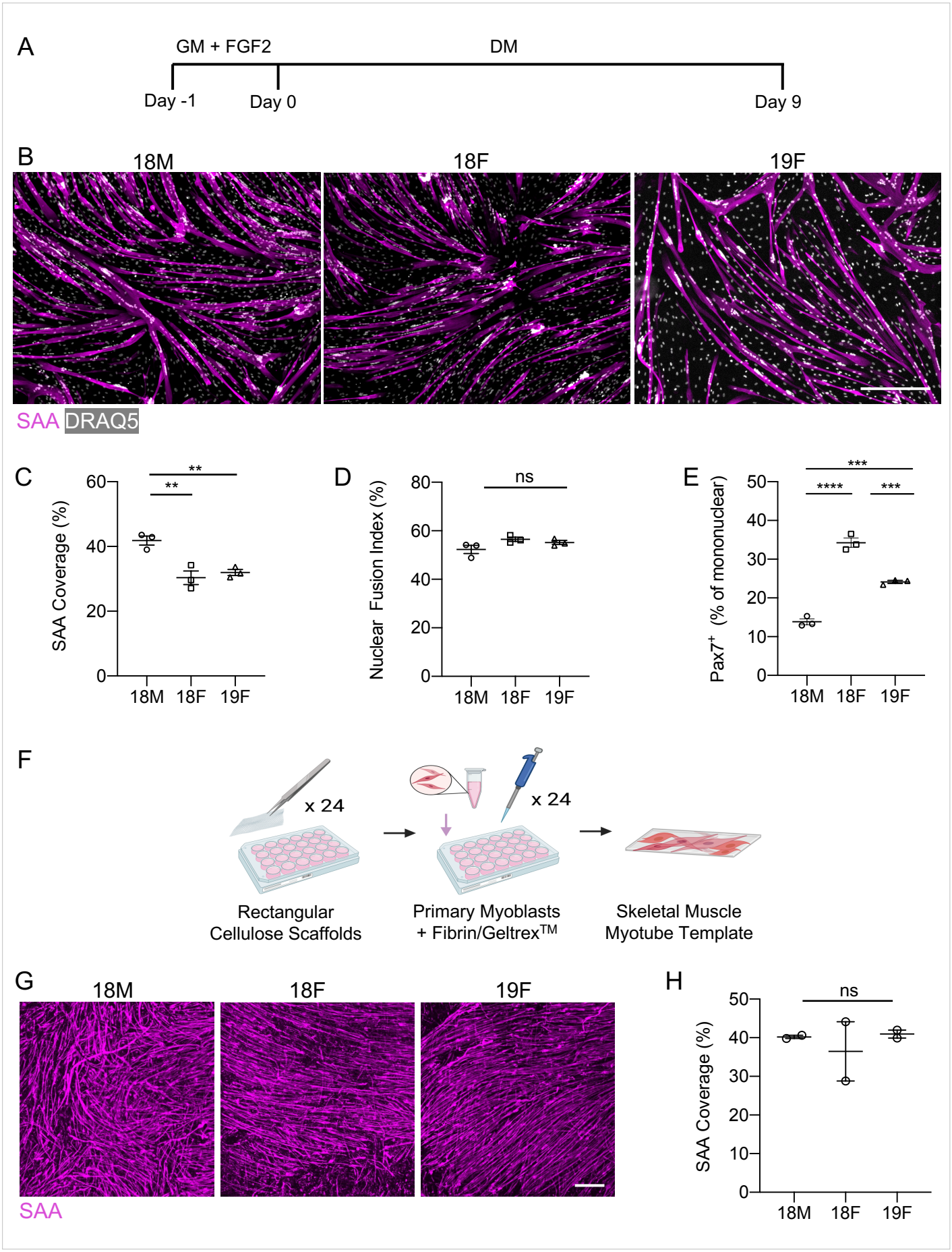
A
GM + FGF2
DM
Day -1
Day 0
Day 9
B
18M
18F
19F
SAA DRAQ5
C
SAA Coverage (%)
60
40
20
0
**
**
18M 18F 19F
D
Nuclear Fusion Index (%)
80
60
40
20
0
ns
18M 18F 19F
E
Pax7+ (% of mononuclear)
50
40
30
20
10
0
***
****
***
18M 18F 19F
F
x 24
x 24
Rectangular Cellulose Scaffolds
Primary Myoblasts + Fibrin/Geltrex™
Skeletal Muscle Myotube Template
G
18M
18F
19F
SAA
H
SAA Coverage (%)
50
40
30
20
10
0
ns
18M 18F 19F

Figure 2

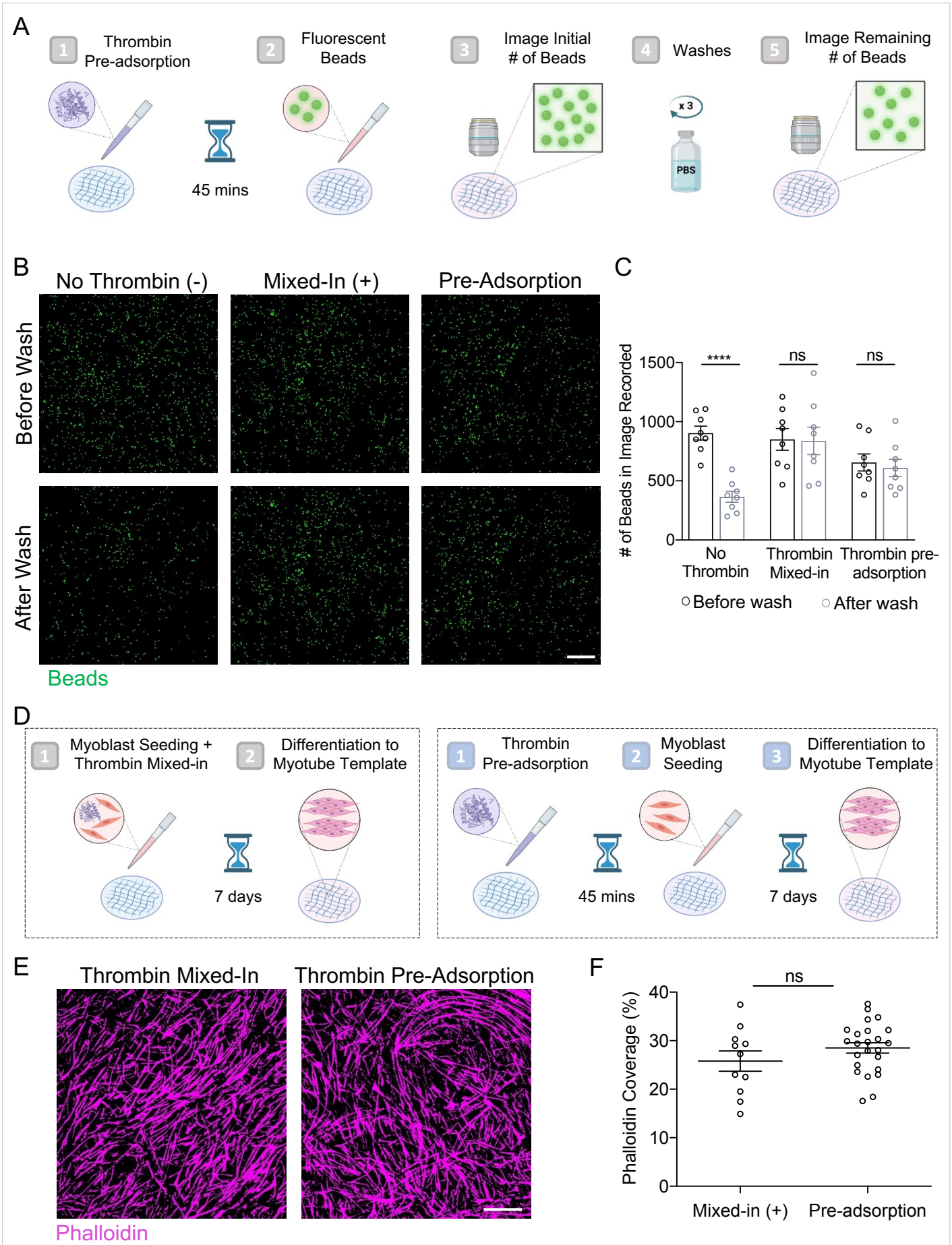
A
1 Thrombin Pre-adsorption
2 Fluorescent Beads
3 Image Initial # of Beads
4 Washes
5 Image Remaining # of Beads
45 mins
x 3
PBS
B
No Thrombin (-)
Mixed-In (+)
Pre-Adsorption
Before Wash
After Wash
Beads
C
# of Beads in Image Recorded
1500
1000
500
0
****
ns
ns
No Thrombin
Thrombin Mixed-in
Thrombin pre-adsorption
Before wash
After wash
D
1 Myoblast Seeding + Thrombin Mixed-in
2 Differentiation to Myotube Template
7 days
1 Thrombin Pre-adsorption
2 Myoblast Seeding
3 Differentiation to Myotube Template
45 mins
7 days
E
Thrombin Mixed-In
Thrombin Pre-Adsorption
Phalloidin
F
ns
Phalloidin Coverage (%)
40
30
20
10
0
Mixed-in (+)
Pre-adsorption

Figure 3

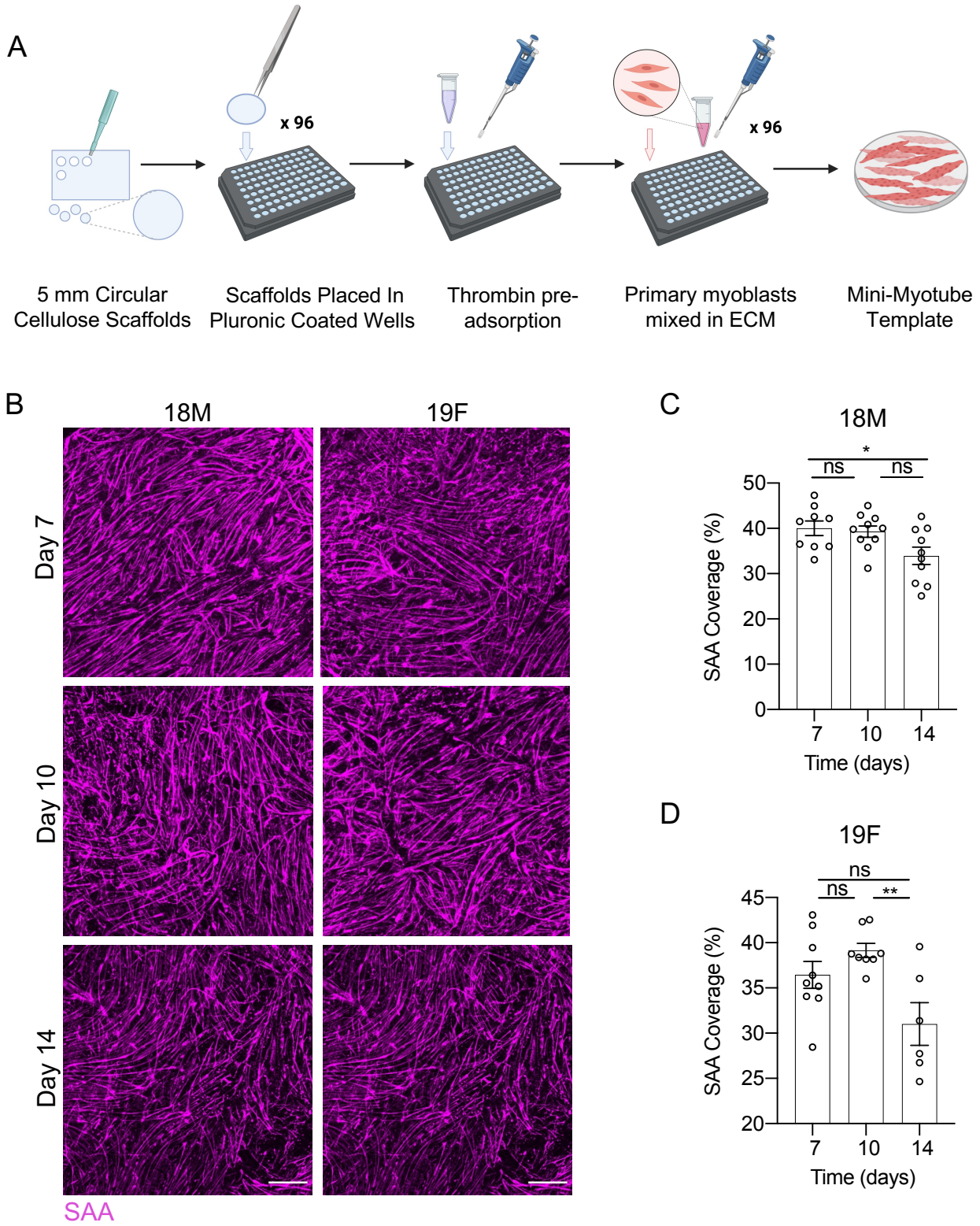
A
x 96
x 96
5 mm Circular Cellulose Scaffolds
Scaffolds Placed In Pluronic Coated Wells
Thrombin pre-adsorption
Primary myoblasts mixed in ECM
Mini-Myotube Template
B
18M
19F
Day 7
Day 10
Day 14
SAA
C
18M
ns
*
ns
SAA Coverage (%)
50
40
30
20
10
0
7
10
14
Time (days)
D
19F
ns
ns
**
SAA Coverage (%)
45
40
35
30
25
20
7
10
14
Time (days)

Figure 4

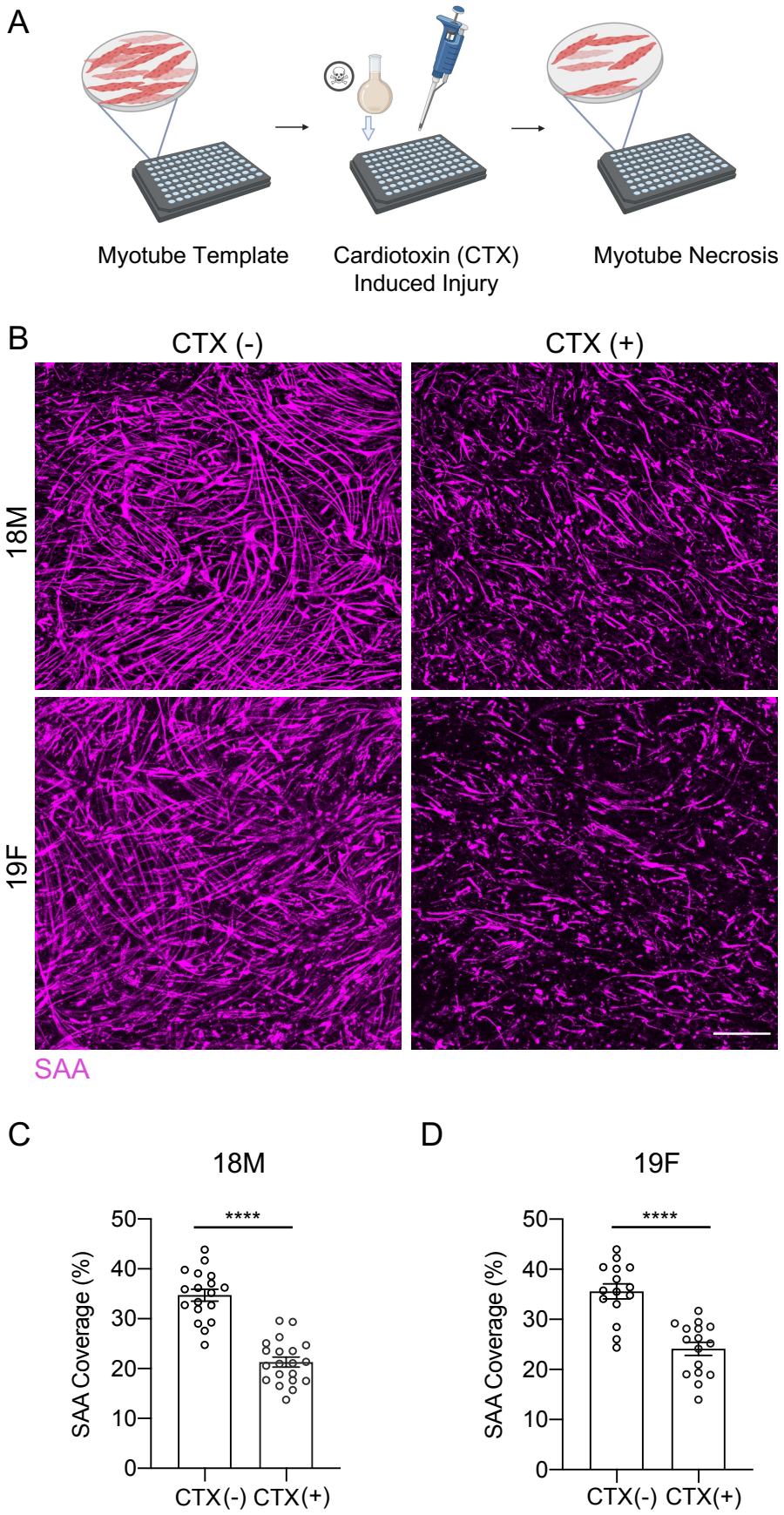
A
Myotube Template
Cardiotoxin (CTX) Induced Injury
Myotube Necrosis
B
CTX (-)
CTX (+)
18M
19F
SAA
C
18M
SAA Coverage (%)
50
40
30
20
10
0
****
CTX(-) CTX(+)
D
19F
SAA Coverage (%)
50
40
30
20
10
0
****
CTX(-) CTX(+)

Figure 5

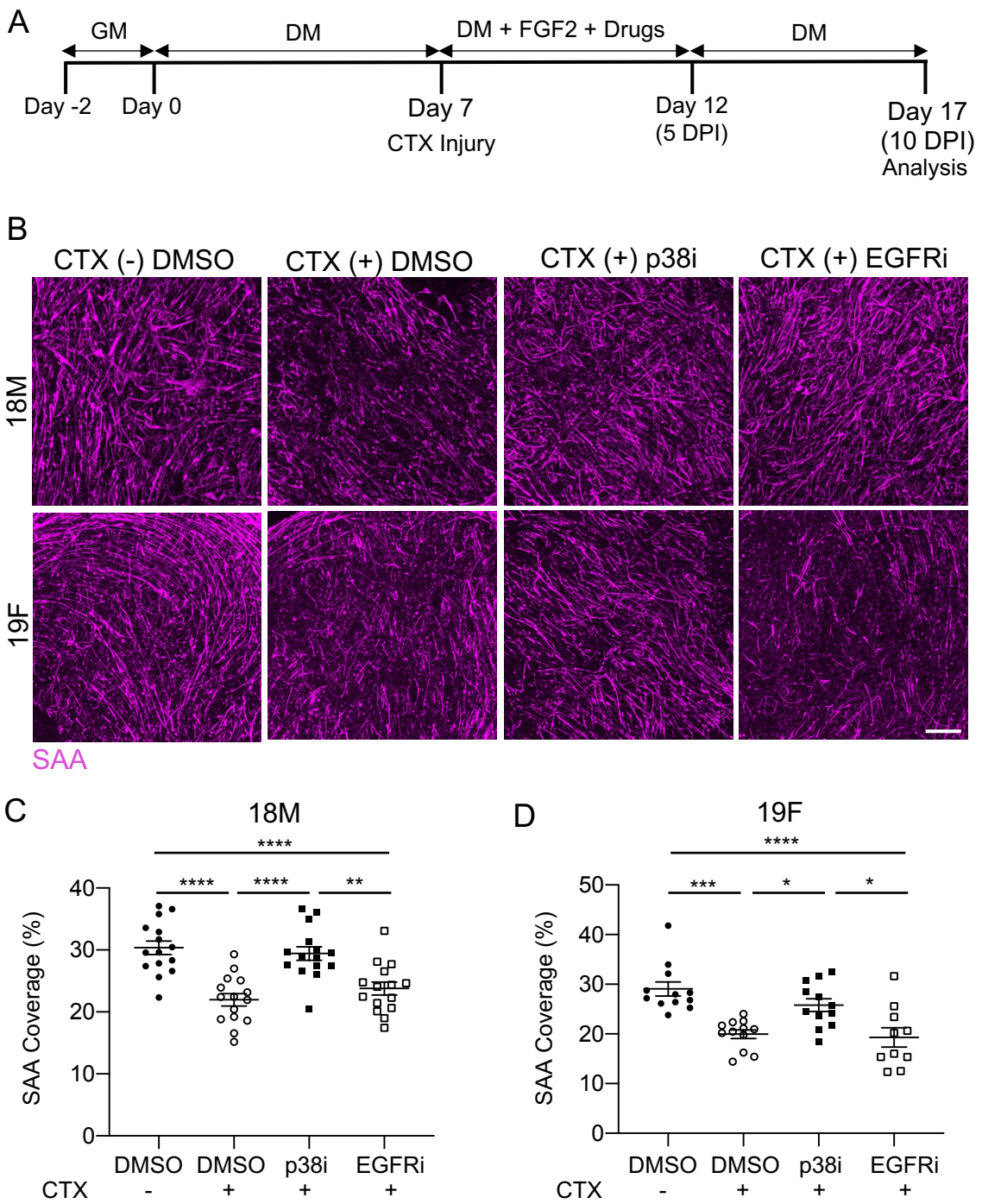
A
GM
DM
DM + FGF2 + Drugs
DM
Day -2
Day 0
Day 7
CTX Injury
Day 12
(5 DPI)
Day 17
(10 DPI)
Analysis
B
CTX (-) DMSO
CTX (+) DMSO
CTX (+) p38i
CTX (+) EGFRi
18M
19F
SAA
C
18M
SAA Coverage (%)
DMSO
DMSO
p38i
EGFRi
CTX
-
+
+
+
D
19F
SAA Coverage (%)
DMSO
DMSO
p38i
EGFRi
CTX
-
+
+
+

Figure 6

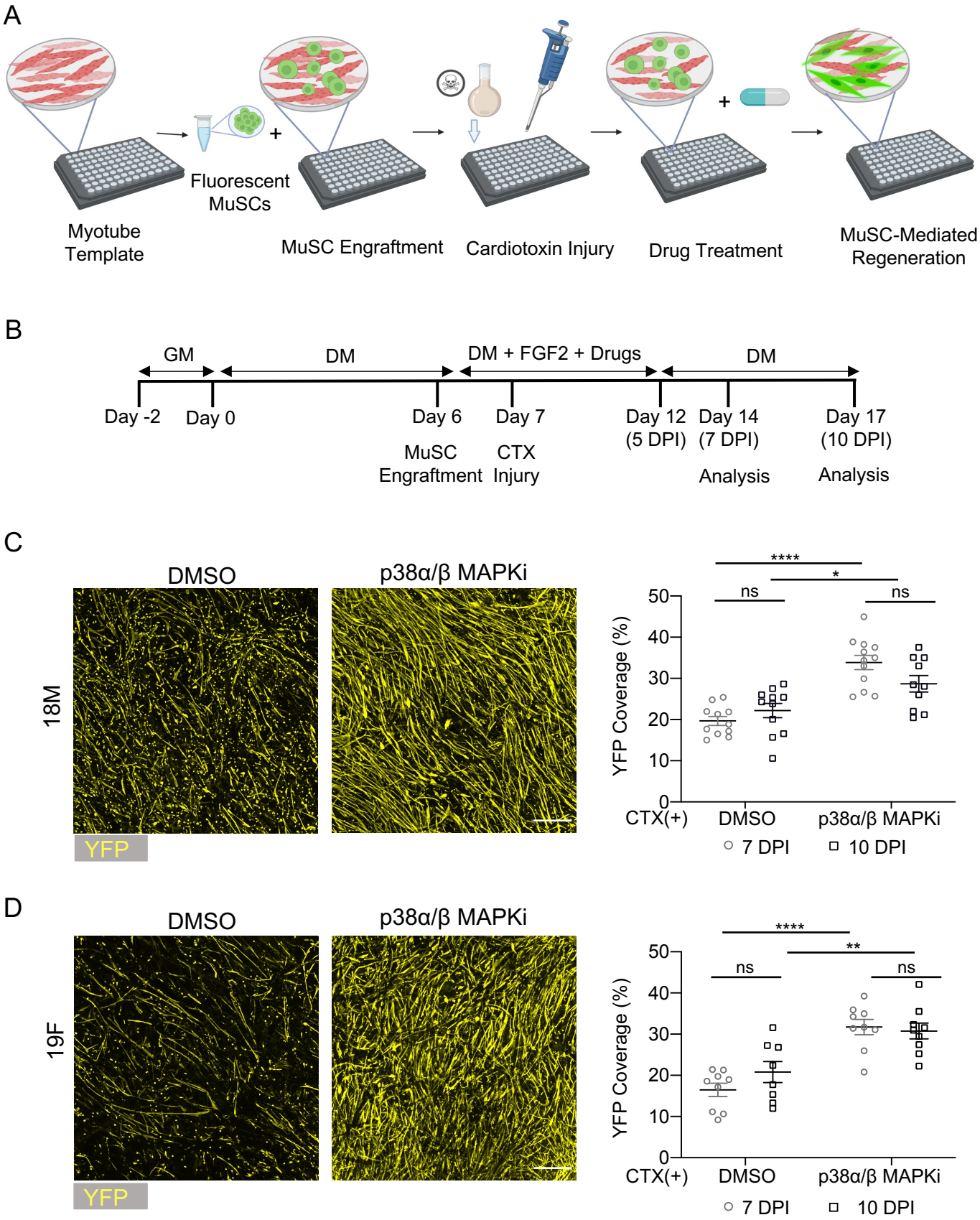
A
Myotube Template
Fluorescent MuSCs
MuSC Engraftment
Cardiotoxin Injury
Drug Treatment
MuSC-Mediated Regeneration
B
GM
DM
DM + FGF2 + Drugs
DM
Day -2
Day 0
Day 6
Day 7
Day 12 (5 DPI)
Day 14 (7 DPI)
Day 17 (10 DPI)
MuSC Engraftment
CTX Injury
Analysis
Analysis
C
DMSO
p38α/β MAPKi
18M
YFP
YFP Coverage (%)
CTX(+)
DMSO
p38α/β MAPKi
7 DPI
10 DPI
ns
****
*
ns
D
DMSO
p38α/β MAPKi
19F
YFP
YFP Coverage (%)
CTX(+)
DMSO
p38α/β MAPKi
7 DPI
10 DPI
ns
****
**
ns

Figure 7

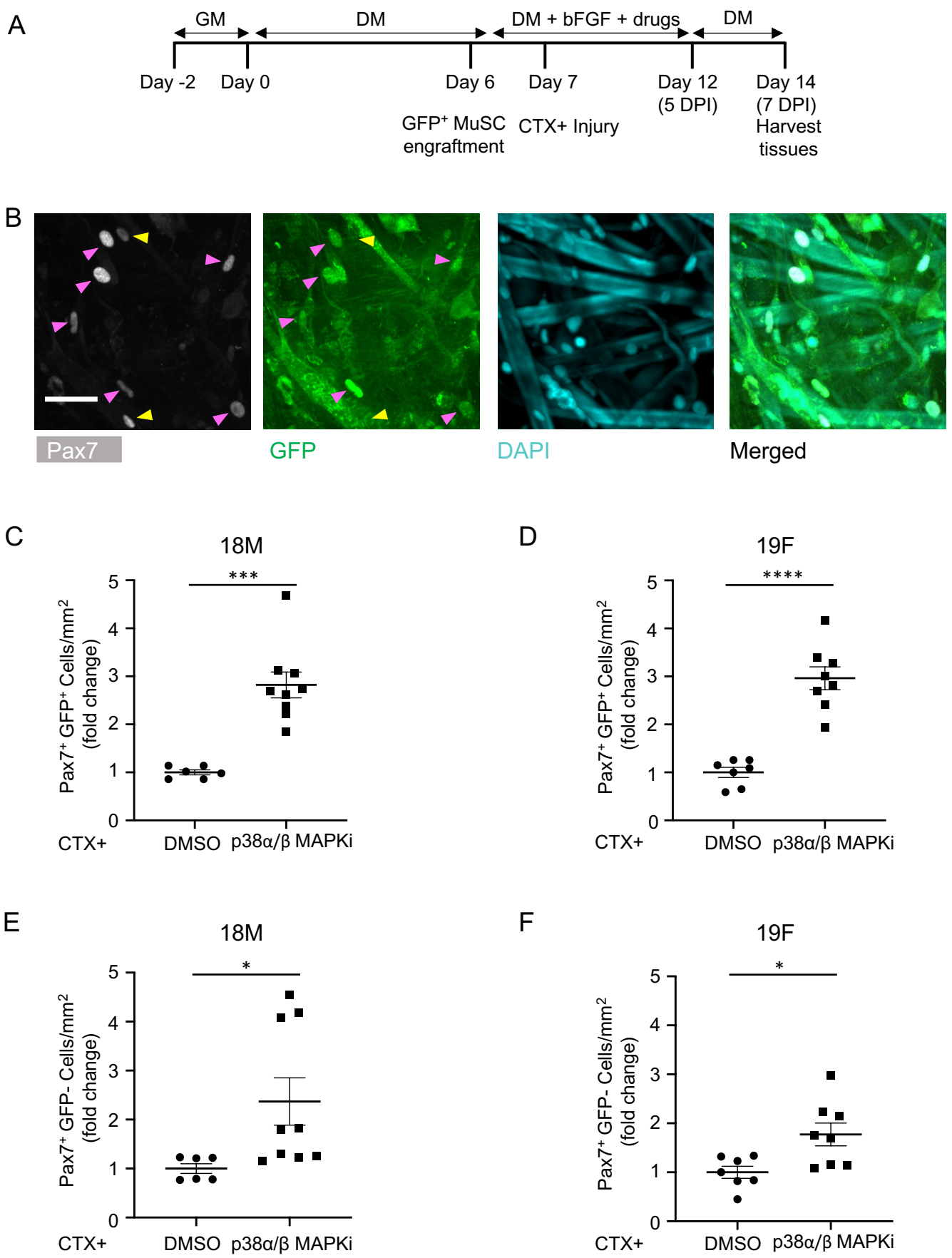
A
GM
DM
DM + bFGF + drugs
DM
Day -2
Day 0
Day 6
Day 7
Day 12
(5 DPI)
Day 14
(7 DPI)
Harvest
tissues
GFP+ MuSC
engraftment
CTX+ Injury
B
Pax7
GFP
DAPI
Merged
C
18M
***
Pax7+ GFP+ Cells/mm2
(fold change)
CTX+
DMSO
p38α/β MAPKi
D
19F
****
Pax7+ GFP+ Cells/mm2
(fold change)
CTX+
DMSO
p38α/β MAPKi
E
18M
*
Pax7+ GFP- Cells/mm2
(fold change)
CTX+
DMSO
p38α/β MAPKi
F
19F
*
Pax7+ GFP- Cells/mm2
(fold change)
CTX+
DMSO
p38α/β MAPKi

Supplementary Figure 1

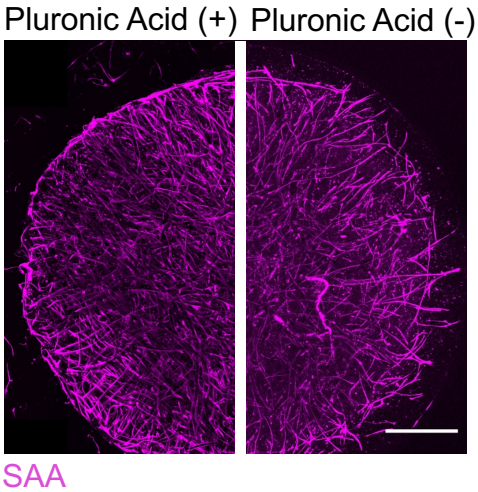

Supplementary Figure 2

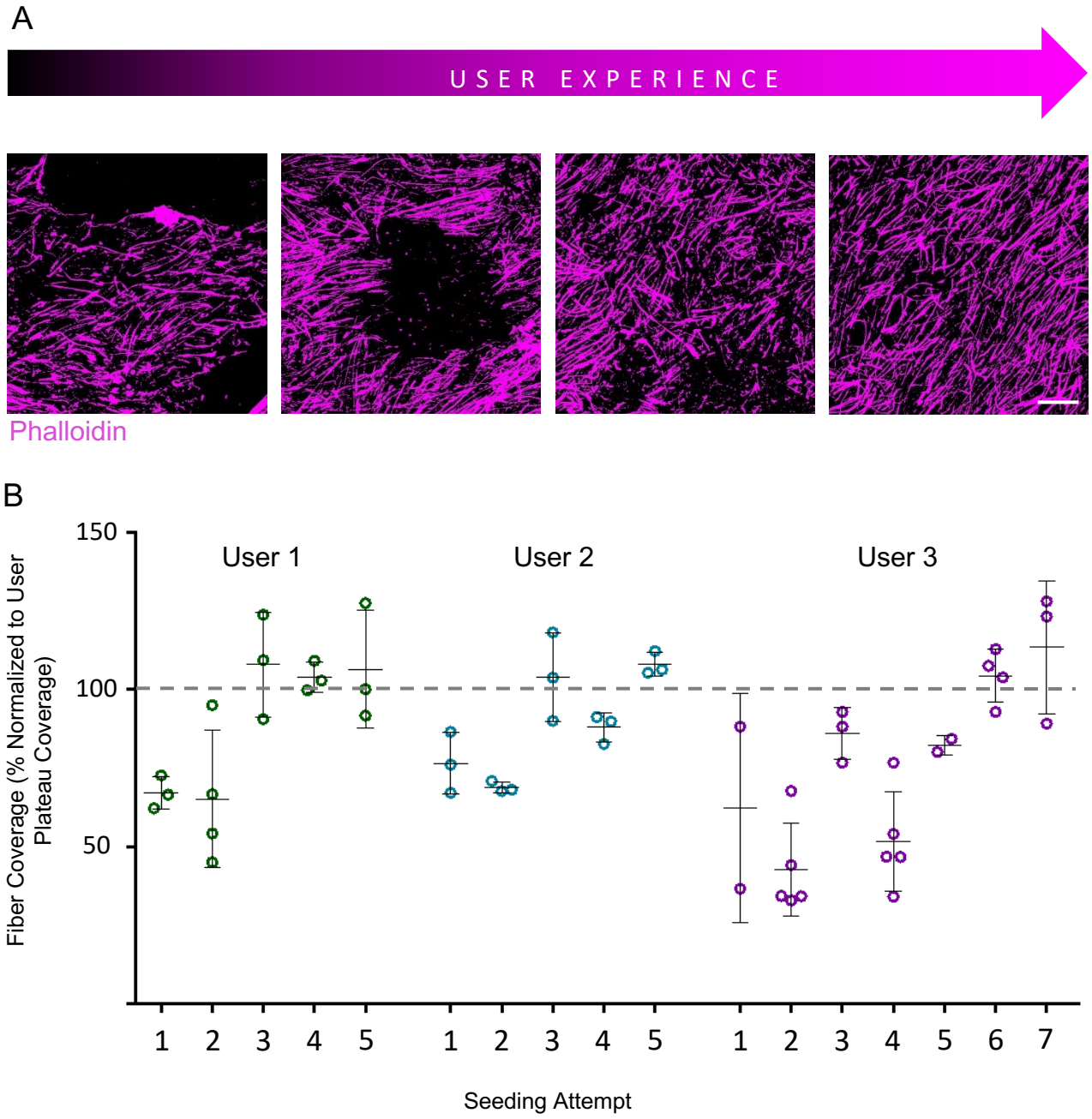

Supplementary Figure 3

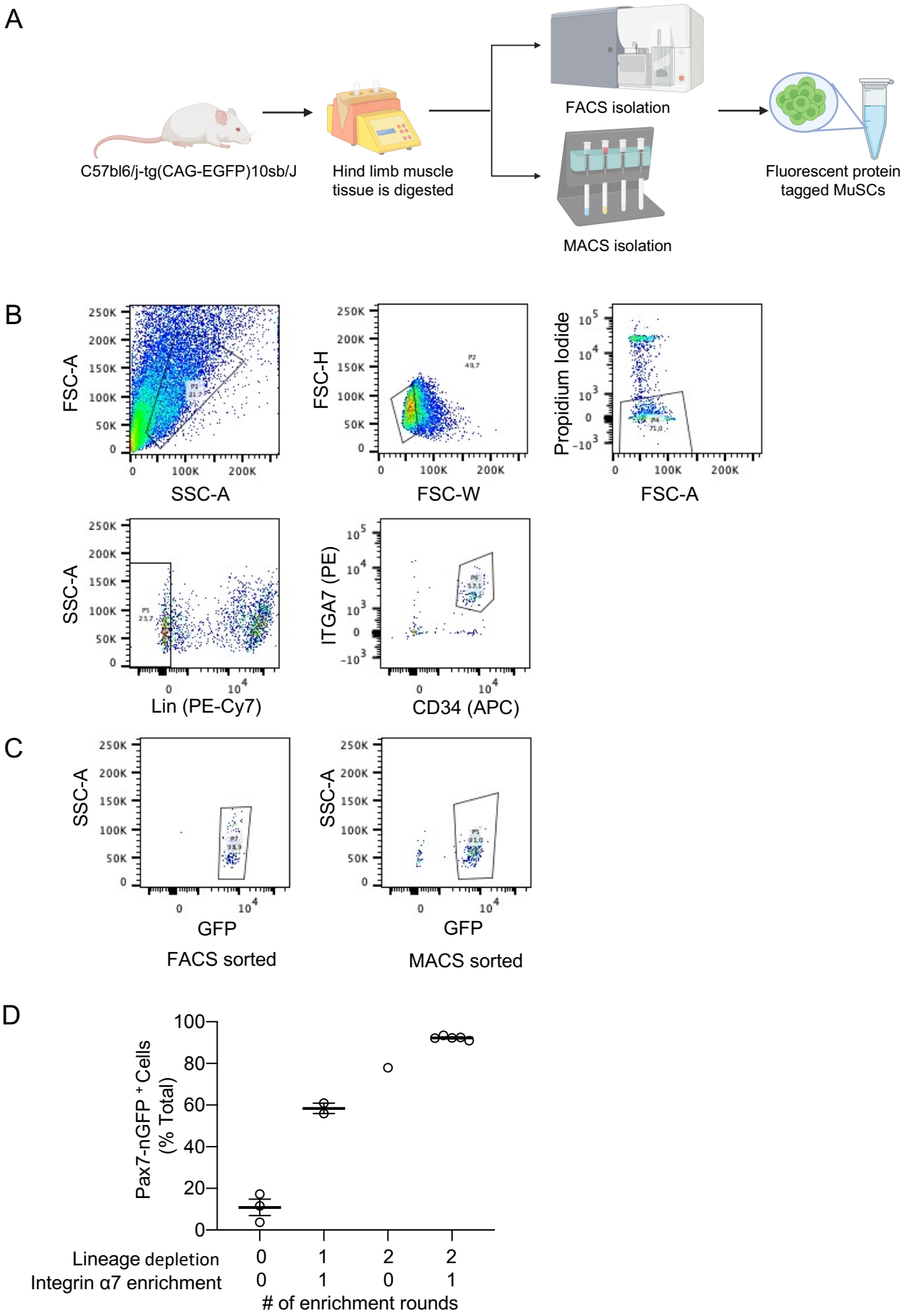
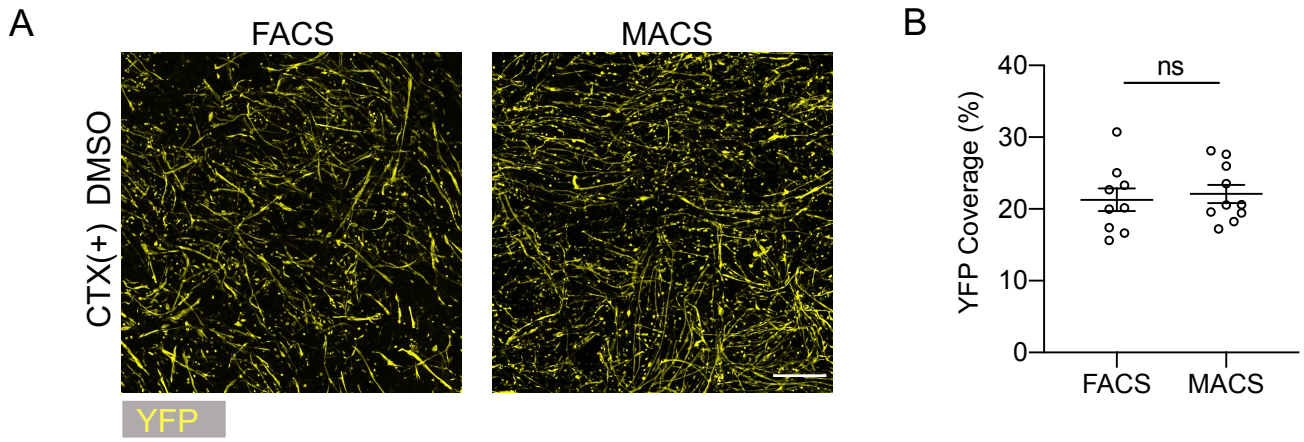
Supplementary Figure 4